TECHNICAL NOTE R-145

EXPERIMENTAL TRANSIENT THREE-DIMENSIONAL HEAT TRANSFER ANALYSIS

by Dr. Roy W. Blanton, Jr.

J. Wayne Littles

May 1965

N66 32715

(ACCESSION NUMBER)

68

(PAGES)

CR-67510

(NASA CR OR TMX OR AD NUMBER)

(THRU)

/

(CODE)

33

(CATEGORY)

RESEARCH LABORATORIES

BROWN ENGINEERING COMPANY, INC.

HUNTSVILLE, ALABAMA

TECHNICAL NOTE R-145

EXPERIMENTAL TRANSIENT THREE-DIMENSIONAL
HEAT TRANSFER ANALYSIS

May, 1965

Prepared For

PROPULSION DIVISION
P&VE LABORATORY
GEORGE C. MARSHALL SPACE FLIGHT CENTER

By

RESEARCH LABORATORIES
BROWN ENGINEERING COMPANY, INC.

Contract No. NAS8-5289

Prepared By

Dr. Roy W. Blanton, Jr.
J. Wayne Littles

ABSTRACT

This report describes the results of a study which was undertaken to compare calculated data from the G.E. General Transient Heat Transfer program with experimental data. The capability of the program to handle a total heat flux input as a function of time was verified.

Approved

R. C. Watson, Jr.
Director of Research

TABLE OF CONTENTS

PRECEDING PAGE BLANK NOT FILMED.

LIST OF FIGURES

INTRODUCTION

In order to verify the calculated values for the G. E. General Transient
Heat Transfer program, a study was undertaken to compare calculated data
with data obtained experimentally.

An aluminum channel was used as a specimen and was instrumented
with iron-constantan thermocouples at specified locations. A bank of General
Electric quartz T-3 230 volt infrared lamps was used as an energy source
and the energy output was recorded by use of an asymptotic calorimeter. A
number of tests were run during which the outputs of the thermocouples and
calorimeter were recorded.

A computer model was developed and boundary conditions obtained
during tests were input for several cases. The calculated and experimental
results were compared and the capability of the program to handle total heat
flux boundary condition as a function of time was verified.

EXPERIMENTAL APPARATUS

In order to verify the results of the G. E. General Transient Heat Transfer program, it was requested that experimental measurements of the temperature history at specified points along a 4" X 2" X 14" aluminum channel be compared with the analytically determined history. A specimen was obtained and iron-constantan thermocouples were located on the specimen as depicted in Figure 1. The thermocouples were attached by drilling small holes into the specimen surface, placing the thermocouple bead into the holes, and peening the surface around the holes. A two square inch area located in the center of one leg of the channel was selected to be the portion of the specimen exposed to a radiant heat source. This area was cleaned and blacked with smoke from the burning of spirits of camphor on an asbestos wick (see Figure 2).

The total heat input history was recorded by use of an asymptotic calorimeter. For the first series of tests, the calorimeter was mounted in a block of glass rock insulation. A two inch square area of the glass rock with the heat sensor located at its center, was also blacked (see Figure 2). During tests off-gassing eroded the blacking on the glass rock support and the resulting change in emissivity caused a change in the shape factor. The change in shape factor resulted in a higher heat flux upon the sensor than was present on the specimen (see Appendix B). In order to eliminate this error, the sensor was mounted in an aluminum channel identical to the specimen for a second series of tests (see Figure 3).

It was desired to insulate the specimen on all surfaces other than the two square inch area to be exposed to the heat source. In order to accomplish this and to produce equivalent shape factors for the specimen and heat sensor, the specimen and sensor were mounted in a box and rock wool insulation was packed around them. The exposed surface of the specimen and the sensor face were each placed two inches below the top of the box and located

Irradiated Area

Scale: 1:2

A   A

B   B

C   C

7   6

3 1

4 2

5

Section A-A

14 15

Section B-B

13 12

8

9 10

11

Section C-C
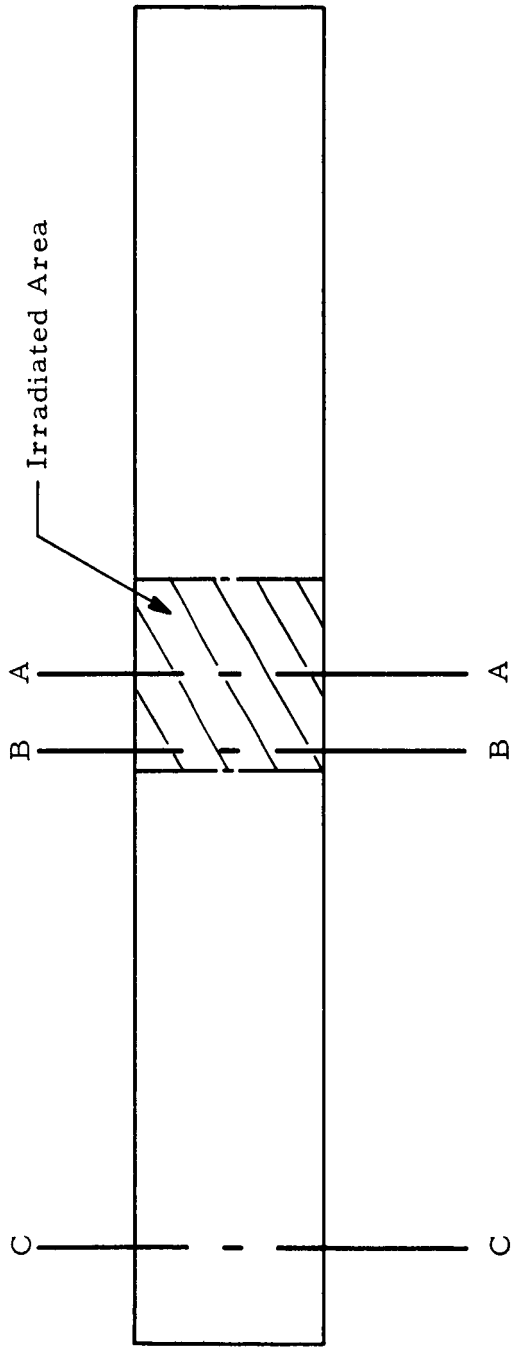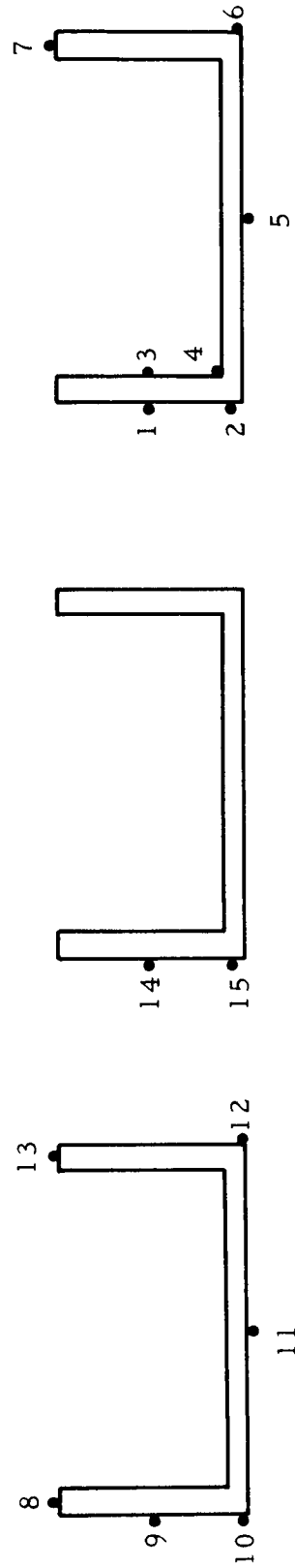
Figure 1. Specimen Thermocouple Locations

4
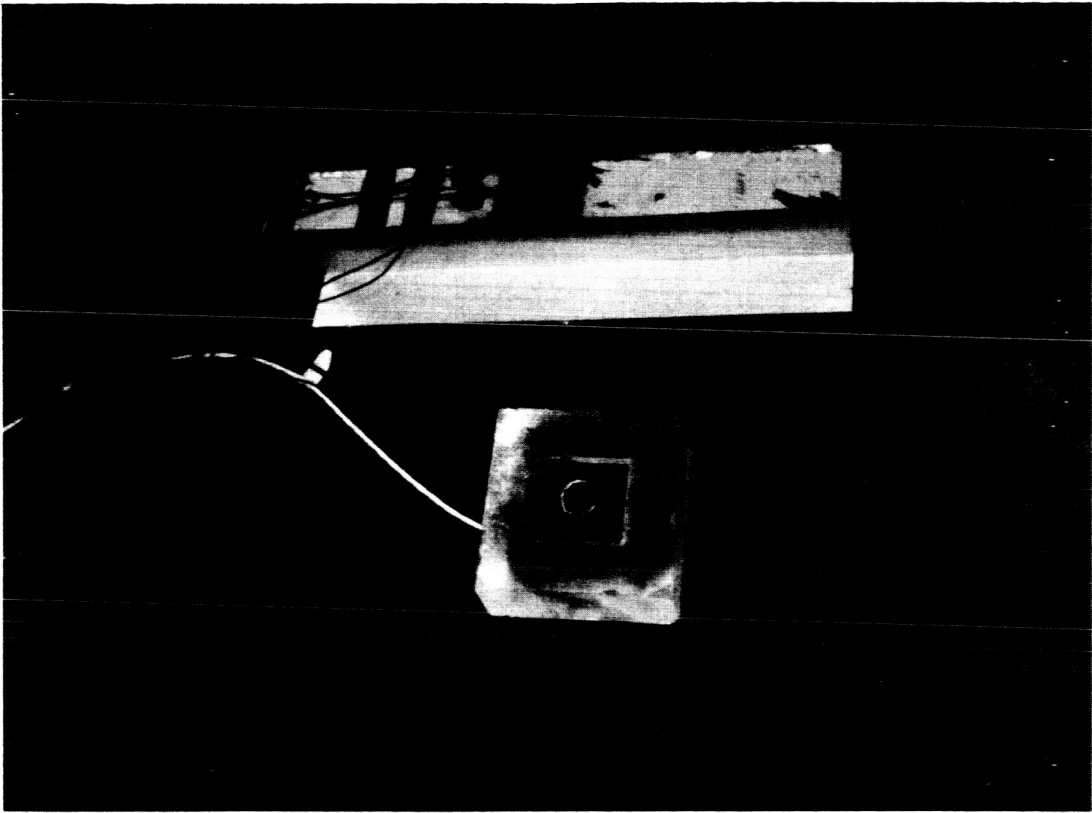
Figure 2. Specimen and Sensor in Glass Rock Mounting
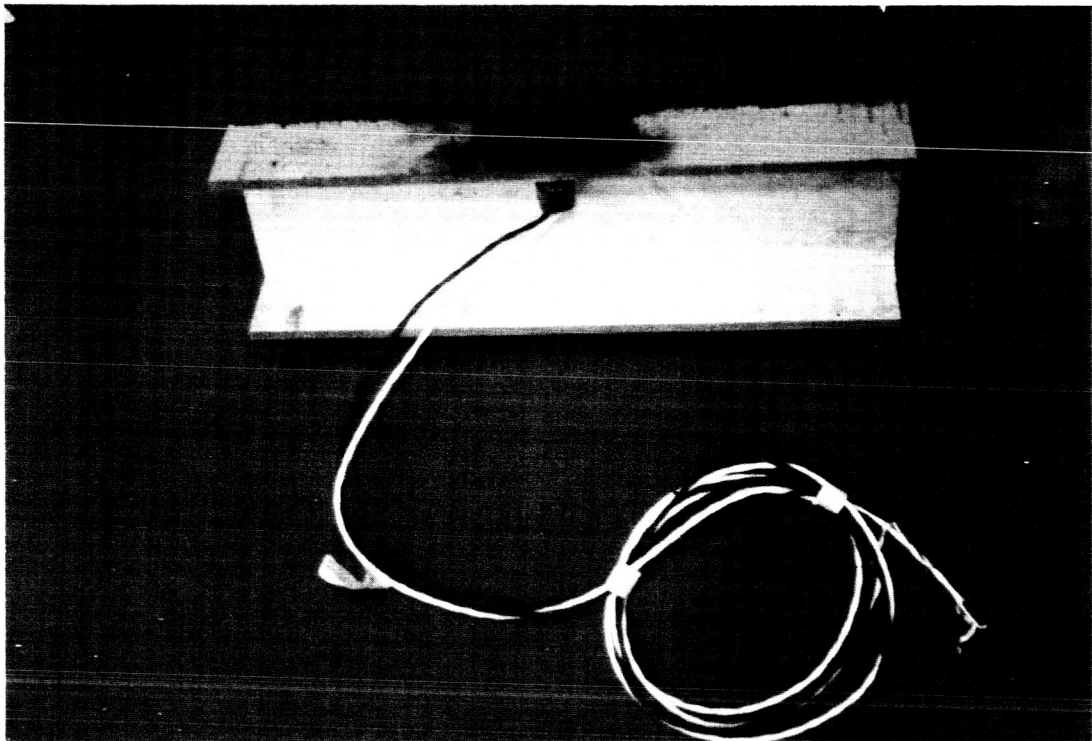
Figure 3. Sensor in Aluminum Channel Mounting

symmetrically with respect to the sides of the box. After the insulation was packed, aluminum foil was also placed over the top of the box to decrease the heat leak through the insulation. It was necessary to replace this foil prior to each test. The final assembly is presented in Figure 4 as it appeared prior to a test.

In order to further assure equivalent shape factors, two square tubes each two inches long were constructed of glass rock insulation and placed over the exposed specimen surface and sensor face, thereby forming two geometrically identical shafts through which the heat flux would pass to the specimen and sensor. The sides of the shafts were lined with aluminum foil.

The heat flux for the tests was provided by a number of 1000 watt T-3 230 volt quartz infrared G. E. lamps. The lamps were shielded on three sides by a stainless steel reflector and mounted on a movable frame (see Figures 5 and 6). This frame allowed the lamps to be positioned above the specimen at any desired height.

The thermocouple outputs were recorded on a 24 point Model 153 Honeywell Electronik multipoint recorder. The EMF output of the heat sensor was recorded on a Honeywell Electronik 17 strip chart recorder. An overall view of the experimental setup is presented in Figure 7.
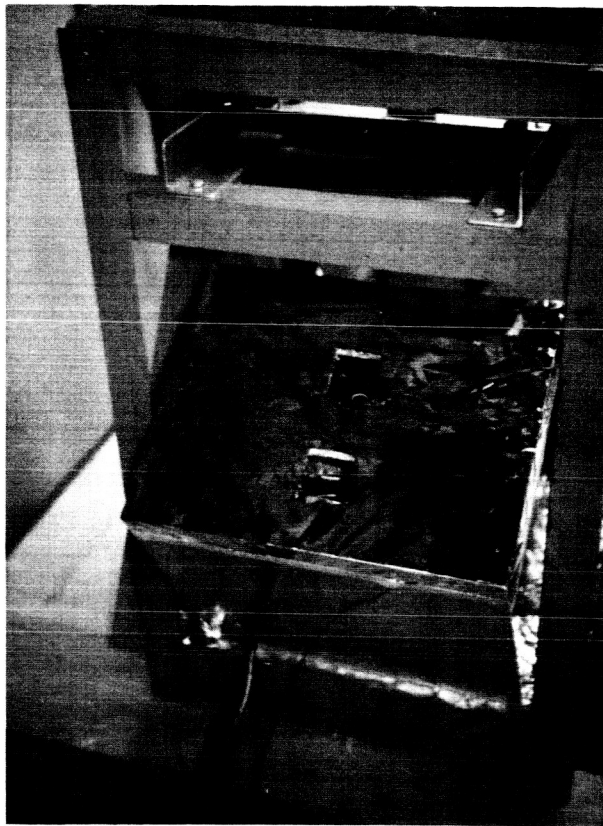
Figure 4. Specimen and Sensor in Insulated Container
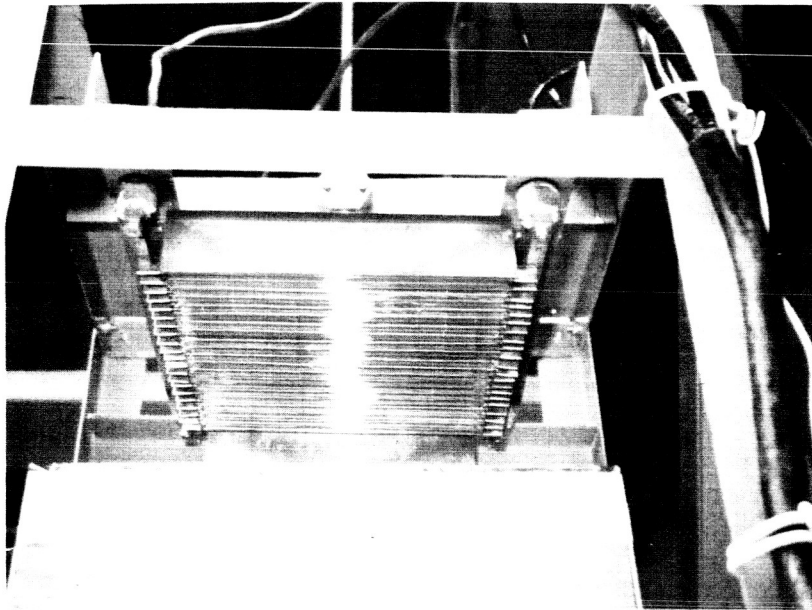
Figure 5. Infrared Lamps and Heat Shield
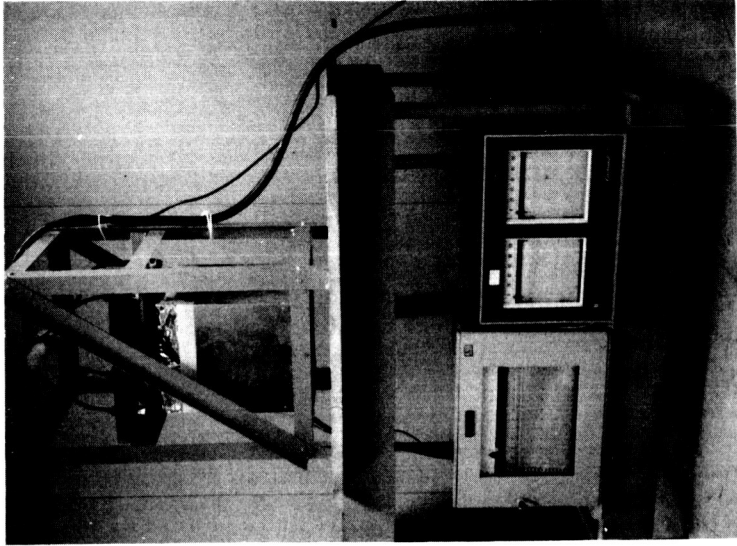
Figure 7. Overall View of Experimental Apparatus
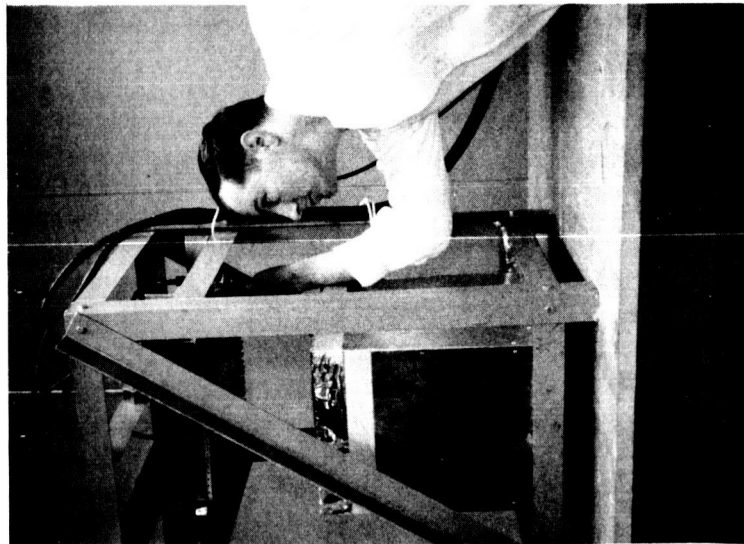
Figure 6. Final Assembly

8

EXPERIMENTAL PROCEDURE

After the specimen and sensor were assembled as shown in Figure 4, the assembly was positioned as shown in Figure 6. Care was taken to assure identical positioning prior to each test. The height of the lamps was adjusted to approximately two inches above the top of the insulation prior to the first test. The frame assembly was leveled and holes for dowel pins were drilled. Prior to each subsequent test the dowel pins were reinserted.

After the recorders had been allowed to warm up, zero readings were taken on the multipoint recorder by allowing a full cycle of 24 points to be printed. The recorder was stopped prior to printing point number one (representing thermocouple number one) in order to give a known reference point for each test. The strip chart record pens were checked for zero positioning and the chart drives engaged.

The tests were begun by turning the lamp power supply and the multipoint recorder on simultaneously. The lamps were allowed to burn for approximately three minutes. It was found that in order to minimize the balance time for the first points after cutoff, the power supply to the lamps should be cut off after point four was printed by the multipoint recorder. The recorders were allowed to run for approximately three minutes after cutoff. After this time the recorders were turned off and the test records were removed from the recorders and dated.

The assembly was allowed to cool for approximately three hours between runs.

DISCUSSION

General

During the period of February 20 to February 22, 1965, initial tests were conducted on the 3-D heat transfer experimental model. Six sets of experimental data were obtained during this period of time. The maximum test duration was 385 seconds and the maximum heat flux was 15 Btu/ft^{2}sec. Analysis of the experimental data indicated that repeatability had been obtained within experimental limits. However, when these data were compared with the values obtained from the G.E. computer program (with the experimentally measured boundary conditions as input data), deviations were found. The calculated temperatures were, in all cases, greater than the experimentally observed temperatures.

A careful examination of the entire procedure for major sources of error revealed three possible ones. Verification of the material properties of the specimen for use in the computer program was needed. A sample was sent to Spectro-Chemical Research Laboratories, Inc. for a spectrographic analysis and the material was determined to be 6061 aluminum alloy. The thermophysical properties for this alloy were obtained from data given in Reference 1. The thermal conductivity as a function of temperature (see Figure 8) was estimated by noting the general effect of the major alloying elements upon thermal conductivity. The initial value was obtained from data given in Reference 2.

The specific heat of an alloy is essentially a weighted average of the specific heats of each element. Since this alloy was approximately 98% aluminum, the specific heat of pure aluminum as a function of temperature (see Figure 9) as given in Reference 1 was used in the computer program.

A second possible source of error was the heat sensor calibration. After receiving the sensor, its surface was blacked with spirits of camphor.
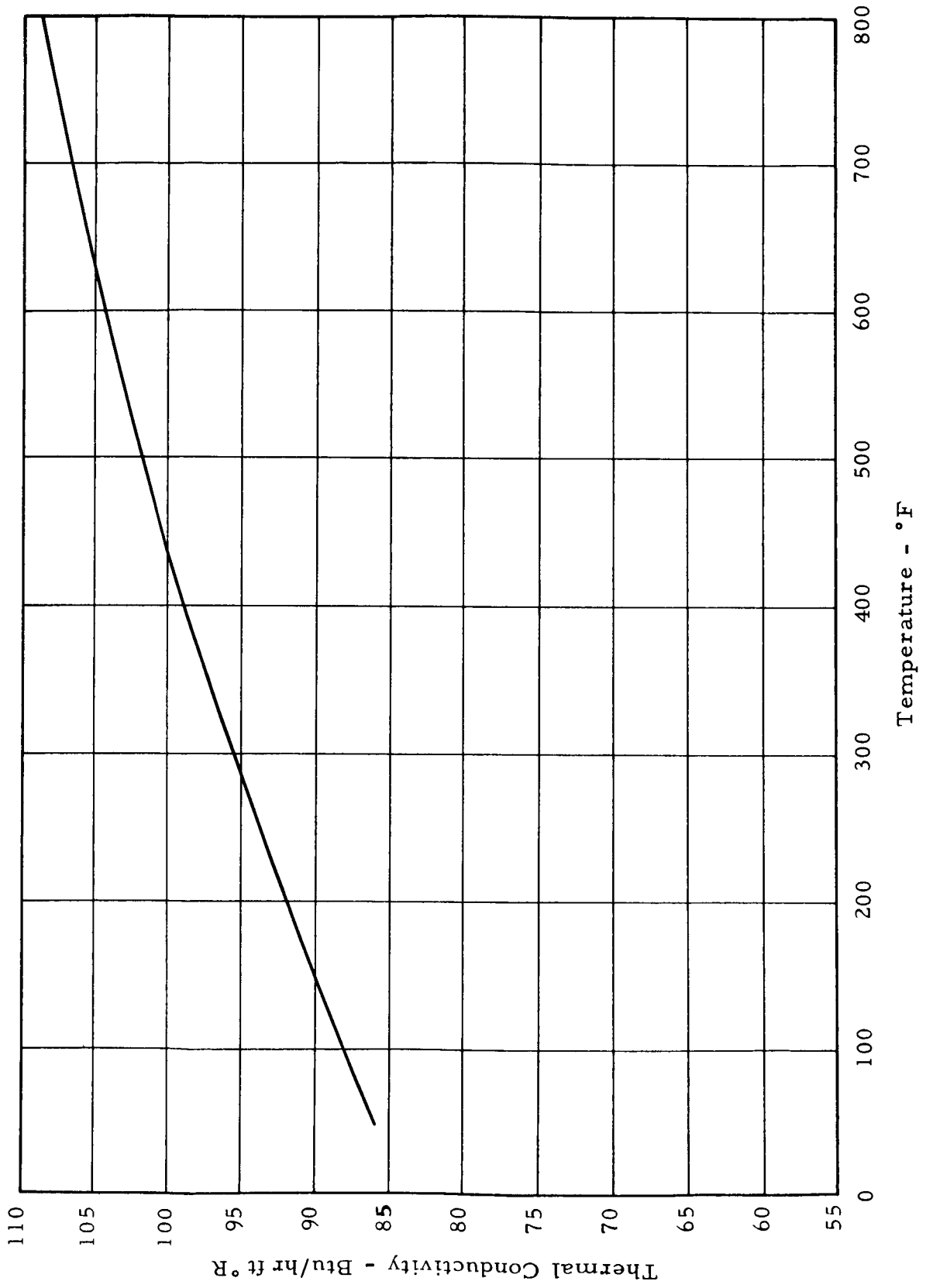
Figure 8. Thermal Conductivity - 6061 Aluminum Alloy
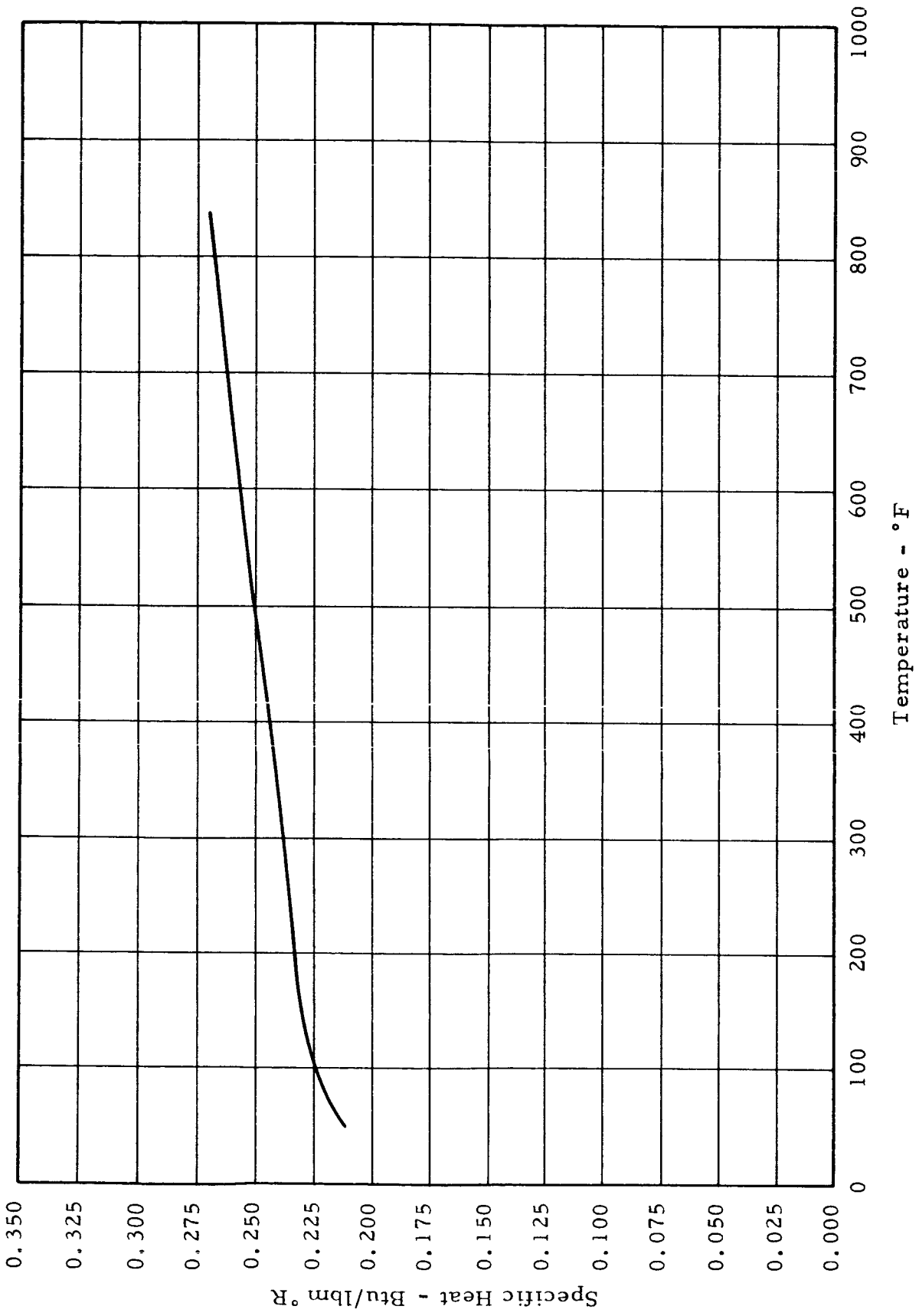
Figure 9. Specific Heat - 6061 Aluminum Alloy

13

A change in the surface emissivity or a change in the sensor sensitivity were possible causes of error. Following the first series of tests, a post-test calibration revealed no significant change over the operating range of these experiments. A comparison of the pretest and posttest calibrations is presented graphically in Figure 10.

A final source of error was a difference between the shape factors for the specimen and the heat sensor. For this series of tests the heat sensor was mounted in a glass rock support (see Figure 2) and the glass rock was blacked prior to tests. Prior to tests, then, the shape factors were equivalent. During tests, however, off-gassing eroded the blacking and changed the emissivity of the surface surrounding the sensor. Shape factor calculations revealed the emissivity of the surface surrounding the sensor to be dominant in determining the value of the shape factor (see Appendix B). The change in the surface emissivity of the glass rock produced a higher heat flux upon the sensor than was present on the specimen.

In order to eliminate the error in the indicated heat flux, a second series of tests were conducted between March 13 and March 15, 1965. To avoid the difficulties presented by the glass rock, the sensor was mounted in an aluminum channel identical to the specimen (see Figure 3). The shape factors for this series remained identical throughout the tests. Analysis of the experimental data revealed excellent repeatability.

Again the measured boundary conditions were input into the G. E. computer program and the resulting data were compared with the experimental data. Agreement was excellent for approximately the first 200 seconds of the tests. After 200 seconds, the calculated values increased more rapidly than the experimental ones. Thermocouples placed in the insulation recorded a slight temperature increase during the tests. In order to isolate the source of this energy, the sensor was placed beneath the insulation at the same level as the specimen. During a four minute test, no measurable heat flux was recorded. Therefore, it was concluded that this energy resulted from a

14
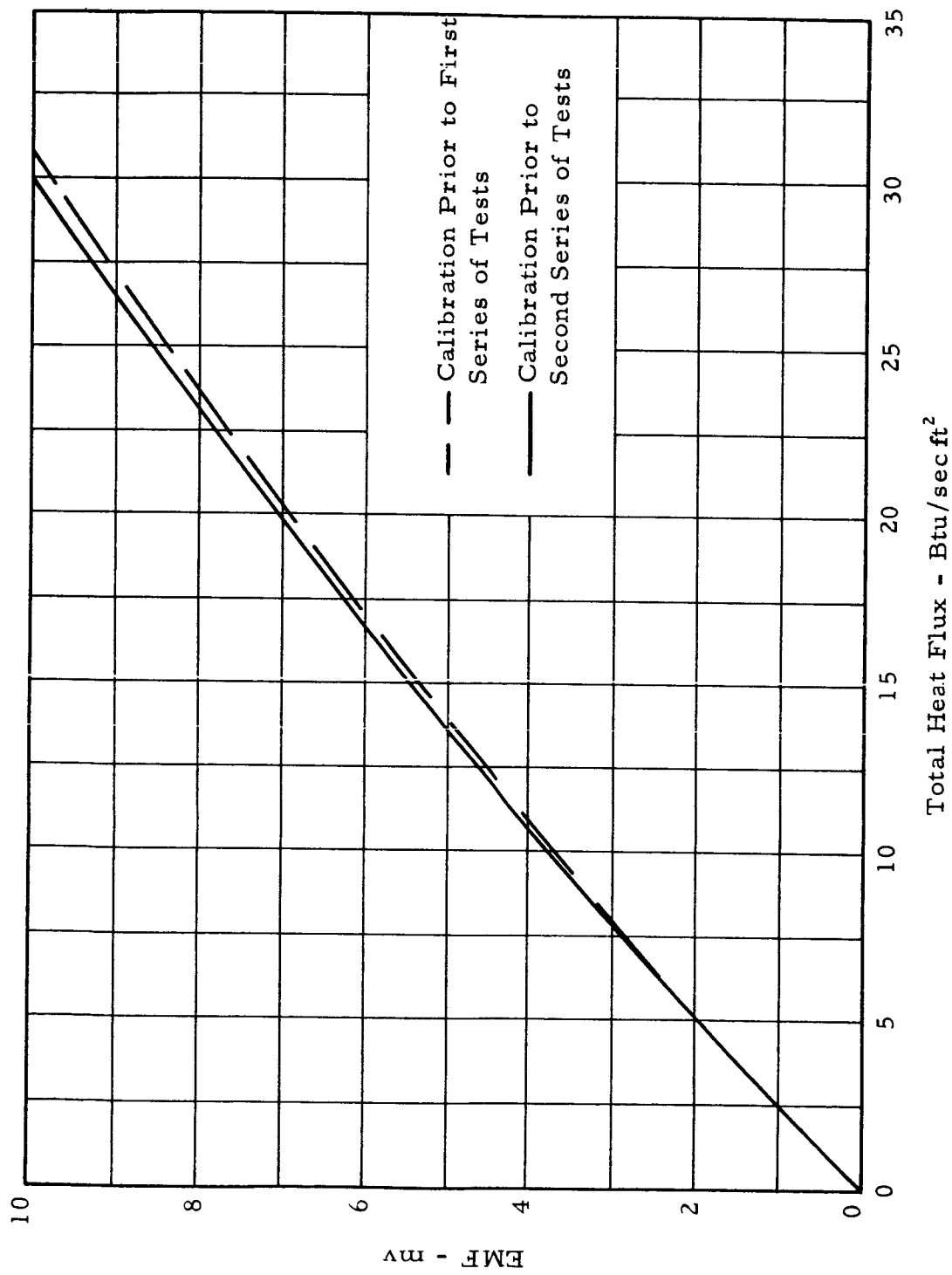
Figure 10. Heat Sensor Calibration

15

specimen heat loss. The model used in the computer program assumed a perfect insulator around the specimen; that is, there were no nodes adjacent to the specimen and the only heat flux to or from it was through the test area. Calculations to estimate the heat loss from the specimen to the insulation, using experimental data, indicated that the energy lost to the insulation could produce a temperature difference in the specimen of the order seen. In order to compensate for this energy loss, the model used in the computer program was modified to include a real insulator at the specimen boundaries.

The results of the modified computer program compare much more favorably with experimental data than did the results of the old model. Comparisons of the results obtained using the two models with each other and with experimental data are presented in Figures 11 and 12.

The modified model was used in all subsequent computer runs. This model utilizes a plane of symmetry which cuts the specimen in half, decreasing the number of nodes needed to describe the specimen geometry and therefore decreasing the required computer time for each run. The modified model includes one inch of rock wool around the specimen (except at the channel end where ideal insulation was assumed and at the ends of the channel legs where one-half inch of rock wool was included). The model utilizes 454 nodes of which 102 are nodes describing the specimen. A schematic diagram of the node system used is presented in Figure 13. The numbering system used in the computer program consisted of prefixing the node number (numbers 01 through 79) with the section number (numbers 0 through 5), thereby producing a three digit number for each node.

Results

The results of the six tests conducted during the last series of tests are presented in Appendix A in graphical and tabular form. The temperature histories of some representative nodes are presented in graphical form and the histories of all other nodes whose temperatures were recorded are presented in tables.

16

Figure 11. Comparison of Real and Ideal Insulation Computer Models (Node 17)

The graph axes and legend read:

Temperature – °F (vertical axis, values: 70, 90, 110, 130, 150, 170, 190, 210)

Time – sec (horizontal axis, values: 0, 40, 80, 120, 160, 200, 240, 280, 320, 360, 400)

Test No. 1

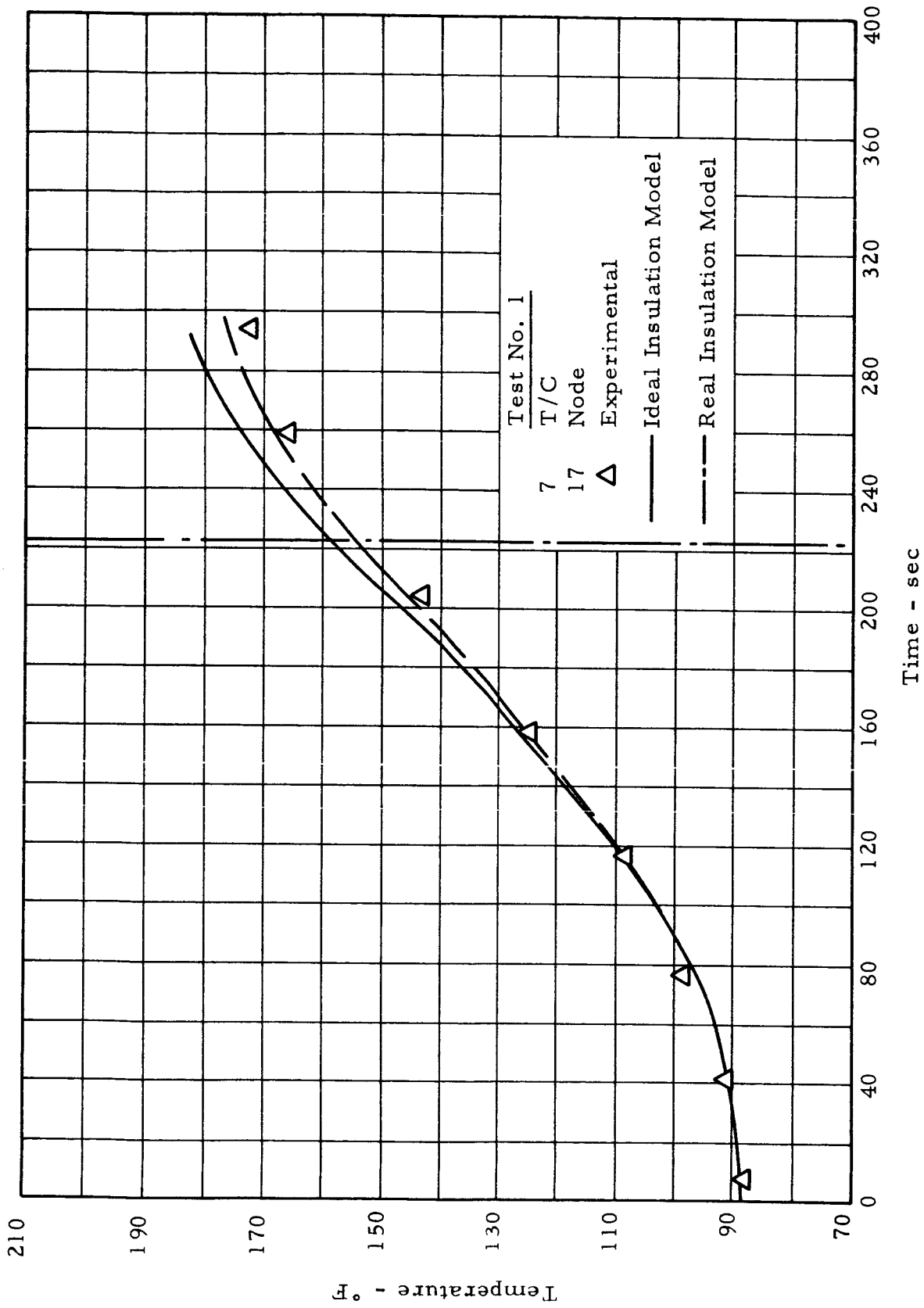| T/C	Node	
7	17	△ Experimental

—— Ideal Insulation Model

—·— Real Insulation Model
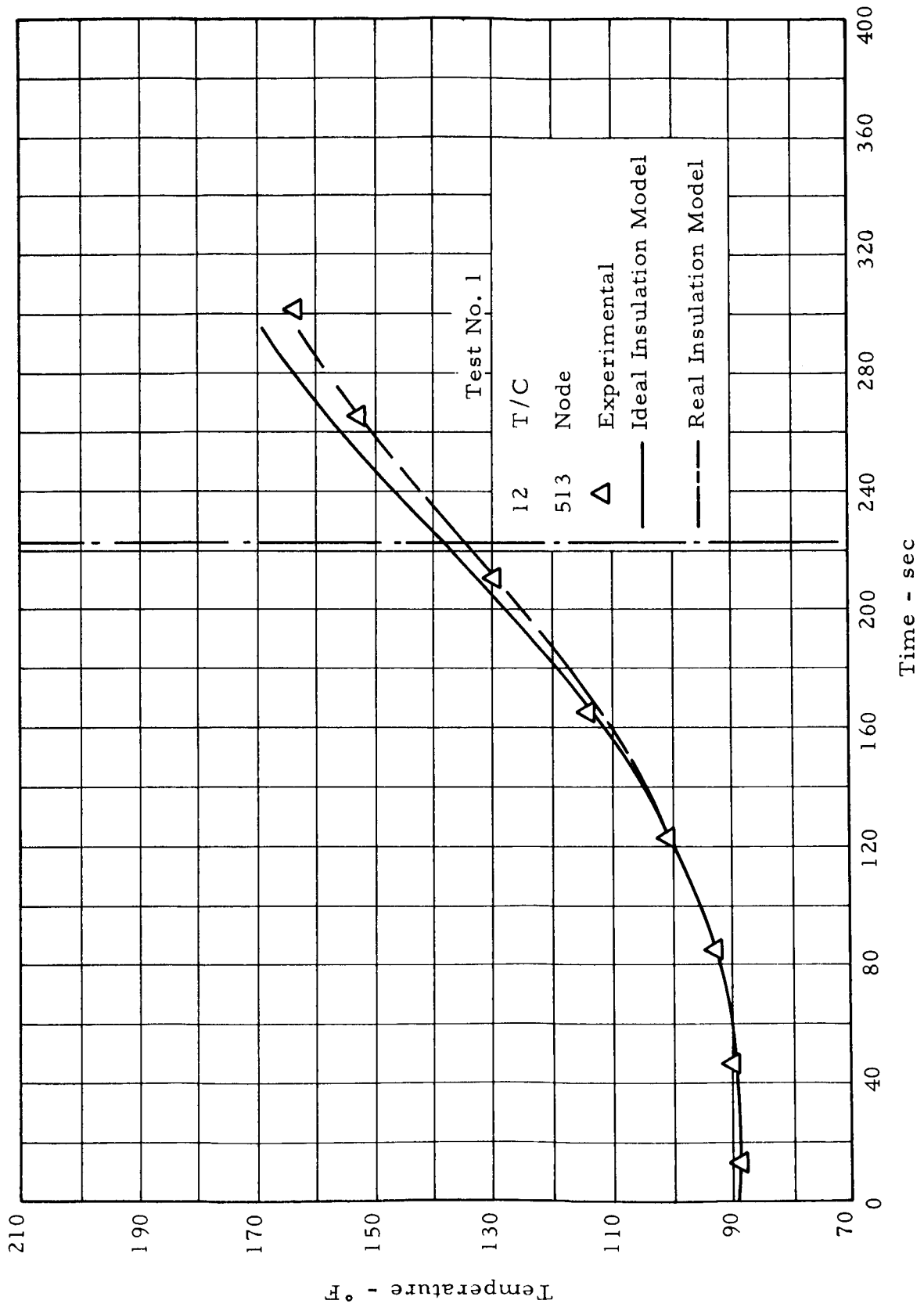
Figure 12. Comparison of Real and Ideal Insulation Computer Models
(Node 513)

18

Top View
Half Scale

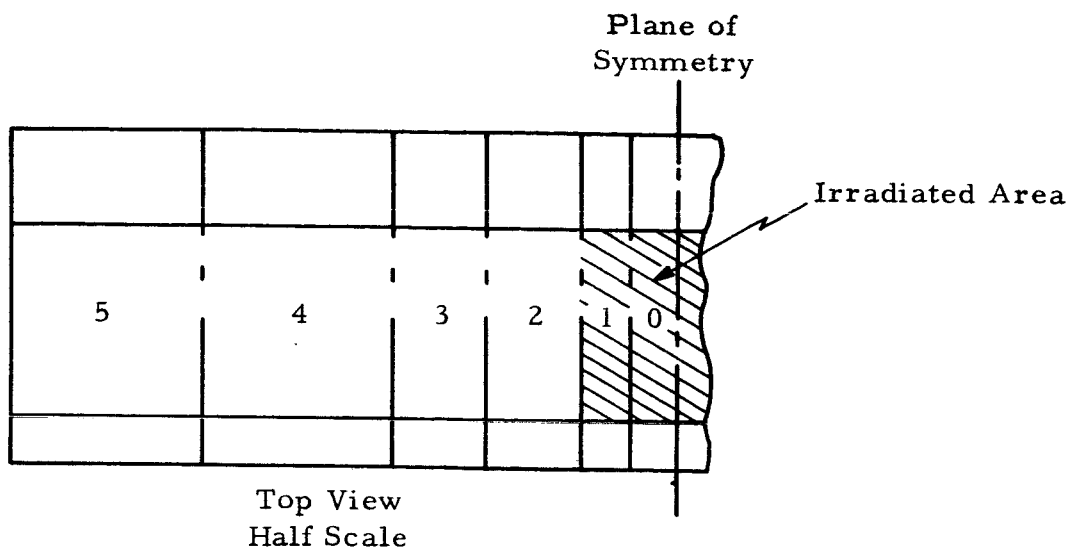Note: Sections "0" and "1" do not have nodes 40-49
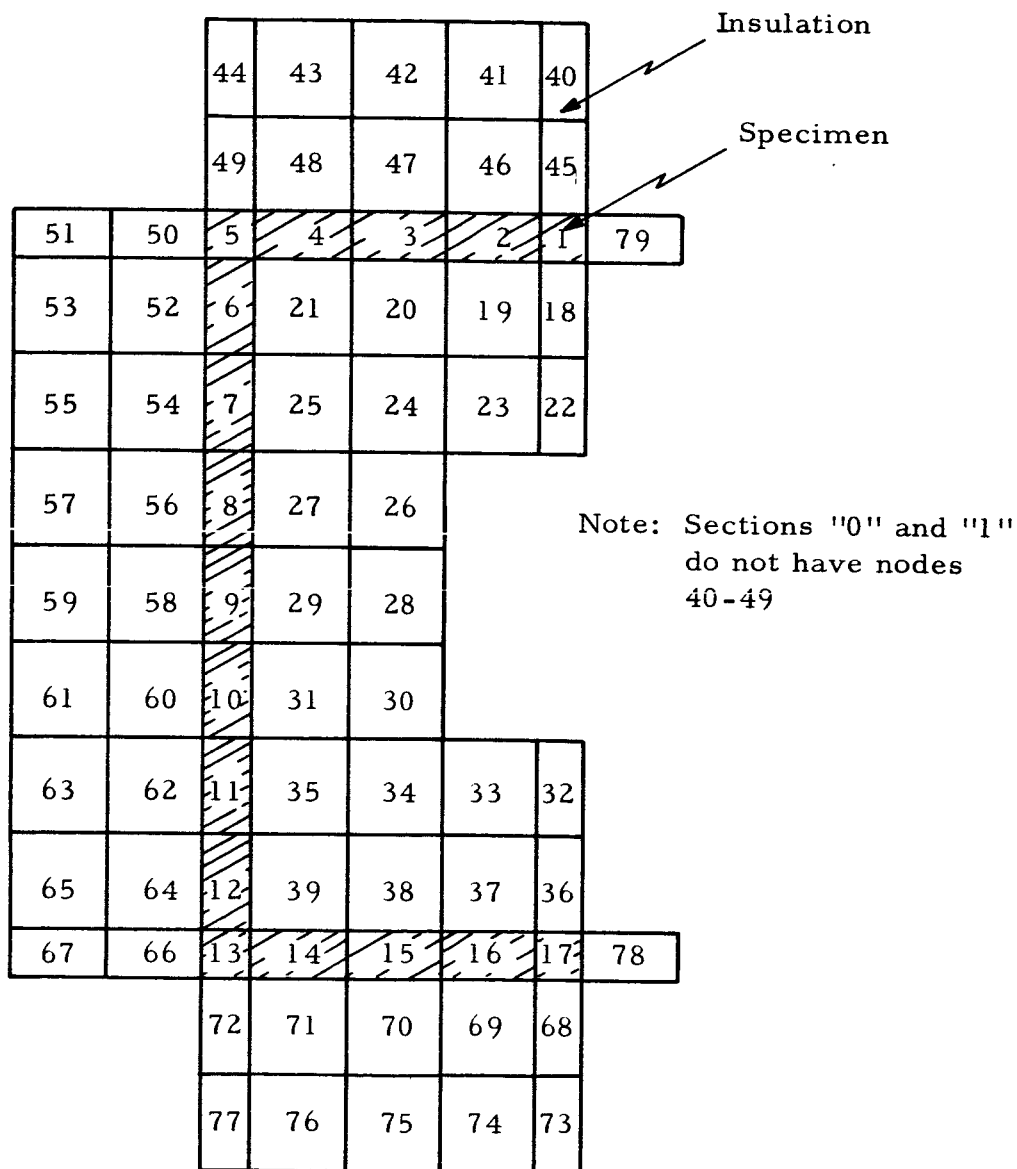
Cross Sections for Sections 2, 3, 4, and 5
Full Scale

Figure 13. Node Configuration

Figures A-1 through A-4 present data for a representative test. In Figure A-1, the variation of heat flux with time is seen. The heat flux produced during this test was typical of that seen during most tests. The increase in heat flux during the test is due primarily to the increase in reradiation from the shield with time. It will be seen that the heat flux was approaching its steady state value as the test was terminated. A comparison of the steady state value during this test with the value predicted in Reference 3 for 230 volt T-3 quartz lamps operating at 208 volts reveals good agreement.

Calculated and experimental temperatures for node three are presented in Figure A-2. As seen in Figure 1, thermocouples one and three were located on the top and bottom respectively of this irradiated node. It would be expected that, due to the large temperature gradient across the node, the calculated value would be the average of these two measured values, as is true after the heat source is turned off. The high experimental values for thermocouple number one from start to cutoff are attributed to direct radiation from the heat lamps to the exposed thermocouple bead.

The results for nodes nine and seventeen are presented in Figure A-3. The experimental results show good agreement with calculated values for both nodes, but are better for node seventeen. However, the agreement for node nine is considered remarkably good when the gradient across the node is considered (see Figure A-5). The accuracy of the calculated results could have been increased by a reduction of node size, but the increase in computation time could not be justified in this case.

Comparison of experimental and calculated data for nodes 501, 509, and 513 are presented in Figure A-4. The deviations are well within the range of experimental error and the agreement is considered excellent.

The data presented in Appendix A are arranged by test and the tests are arranged in chronological order. In addition to the data presented,

experimental data were collected for two other cases. After the second of
these two tests, it was discovered that a quartz lamp located over the speci-
men was faulty. The tube was discovered to have a hole in it and to be dis-
colored. The hole had been caused by a piece of trash falling on the tube
and burning. Since this could have happened during the first of these two
tests, data from both of the tests were excluded. The tube was replaced
after these tests. Two sources of error other than normal experimental
error were observed during the investigation. The heat flux for tests three
and four are seen to decrease from their initial value at the start of the tests.
These decreases are believed to have been caused by voltage fluctuations.
They caused no discernable effect on the results.

Electrical disturbances or equipment sensitivity is believed to have
caused several individual test points to differ more from calculated results
than the same points did during the majority of the tests. Examples of this
are the second and third points for node 509 and the first and second point
for node 513 on test number one, Figure A-4.

Initial computer runs were made using a node configuration which
calculated identical points on both sides of the plane of symmetry. The nodal
arrangement for these runs was similar to that used in the final model
but included the entire specimen. For these runs, it would be expected
that nodes located on opposite ends of the model but symmetrically with
respect to the centerline would have equal temperatures at equal times.
Actually, however, variations of up to 2.5 degrees were seen. These
variations were caused by round-off error during computation and could
have been decreased by reducing the tolerance limit from 0.001 degree.
The additional computation time required was not justifiable for the pur-
poses of this investigation. The deviation seen is, however, a significant
percentage of the difference between experimental and calculated values for
most points.

CONCLUSIONS

The comparison of the experimental data with the calculated results showed excellent correlation for the physical configuration and boundary condition selected for this study.

The mathematical model and temperature tolerance which are selected in the operation of the program affect the results. They will control the total running time of the computer program as well as the accuracy of the results. The convergence of the iteration and thus the roundoff error are directly affected by the temperature tolerance. A variation of up to 2.5 degrees was noted during this investigation for identical points.

REFERENCES

1. Goldsmith, A., T. E. Waterman, and H. J. Hirschborn, "Handbook of Thermophysical Properties of Solid Materials. Volume I: Elements", The Macmillan Company, New York, 1961

2. "Metals Handbook: Volume 1", Eighth edition, American Society for Metals, Metals Park, Ohio, 1961

3. "Product Heating with Infrared Lamps", TP-116, Large Lamp Department, General Electric

4. Fitzgerald, A. E. and D. E. Higginbotham, "Basic Electrical Engineering", Second Edition, McGraw-Hill Book Company, Inc., New York, 1957

5. Holman, J. P., "Heat Transfer", McGraw-Hill Book Company, Inc., New York, 1963

6. Kreith, Frank, "Principles of Heat Transfer", International Textbook Company, Scranton, 1960

APPENDIX A

EXPERIMENTAL AND CALCULATED DATA

TABLE A-1a

Test No. 1

Experimental

T/C/Node	2/5	4/5	6/13	9/503	10/505
Time/Temp	0/88	0/88	0/88	0/88	0/88
Time/Temp	2/102	5/100	7/89	10/88	11/88
Time/Temp	32/168	35/148	39/93	43/91	44/91
Time/Temp	68/210	71/186	75/103	79/99	80/99
Time/Temp	107/262	110/232	113/118	117/113	118/112
Time/Temp	145/300	148/268	152/132	156/126	157/126
Time/Temp	187/336	224/241	228/164	232/160	233/160
Time/Temp	258/219	260/212	263/168	267/167	268/166
Time/Temp	291/202	294/198	297/169	300/169	301/169
Time/Temp	323/192	326/189	329/169	332/170	333/170
Time/Temp	356/186	359/184	362/169	365/170	366/170
Time/Temp	388/182	390/180	393/169	396/170	397/170

TABLE A-1b

Test No. 1

Calculated

| T/C / Node Time	2/5	4/5	6/13	9/503	10/505
0	88	88	88	88	80
20	138	138	88.6	88.2	88.2
40	165.2	165.2	91.8	90.1	89.7
60	190.8	190.8	96.7	93.7	92.9
80	216.6	216.6	102.8	98.8	97.6
100	242.4	242.4	110.1	105.2	103.5
120	266.6	266.6	118.3	112.7	110.5
140	289.6	289.6	127.3	121.1	118.5
160	310.1	310.1	136.9	130.4	127.3
180	328.1	328.1	147.1	140.2	136.8
200	297.5	297.5	157.3	150.4	146.6
220	267.4	267.4	164.8	159.3	155.6
240	245.5	245.5	169.3	165.8	162.4
260	229.8	229.8	172.0	170.0	167.1
280	217.5	217.5	173.6	172.7	170.2
300	206.9	206.9	174.4	174.2	172.1
320	199.2	199.2	174.8	175.0	173.3
340	193.5	193.5	174.8	175.3	173.9
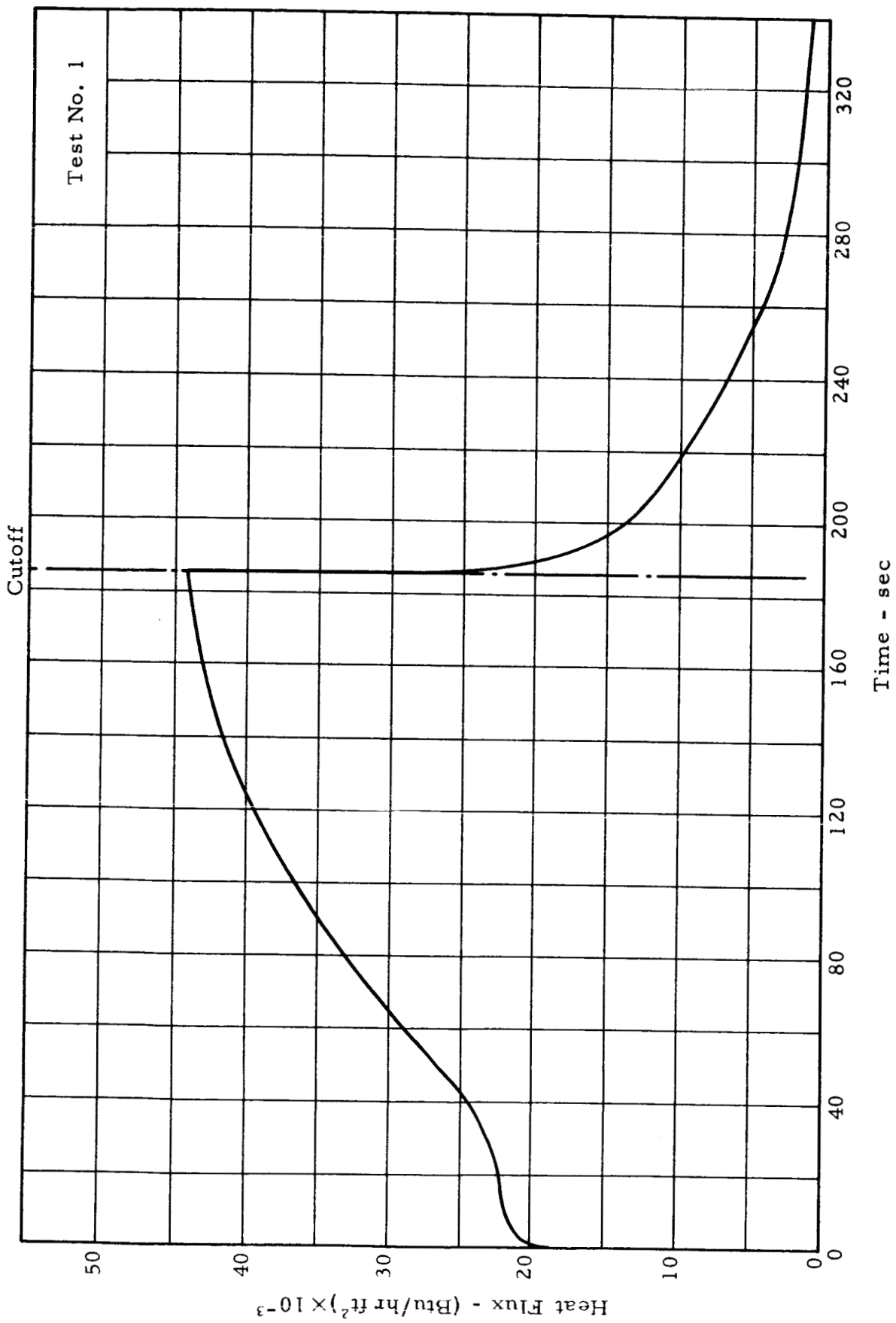
Figure A-1.   Total Heat Flux Versus Time (Test No. 1)
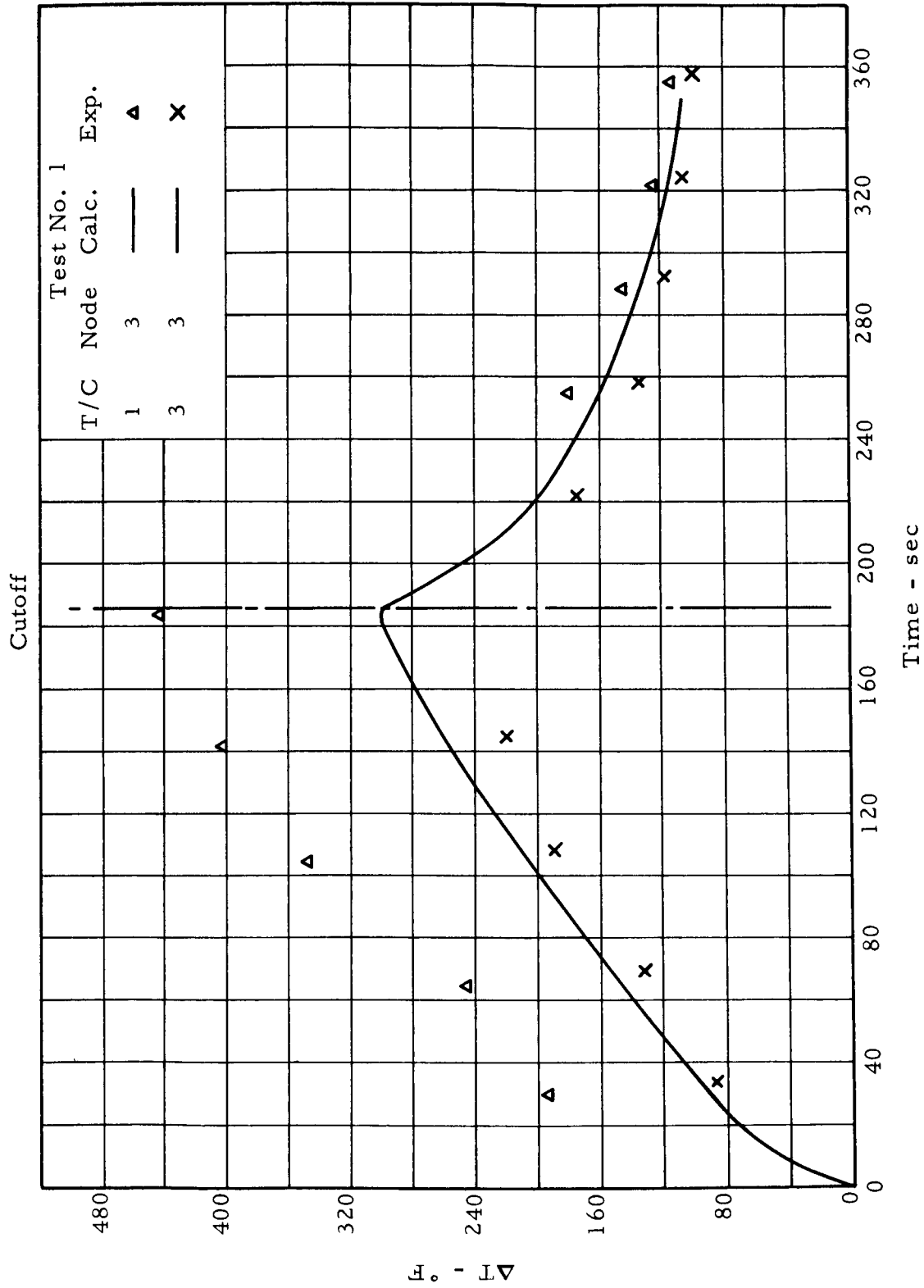
Figure A-2. Temperature Time History (Node 3, Test No. 1)
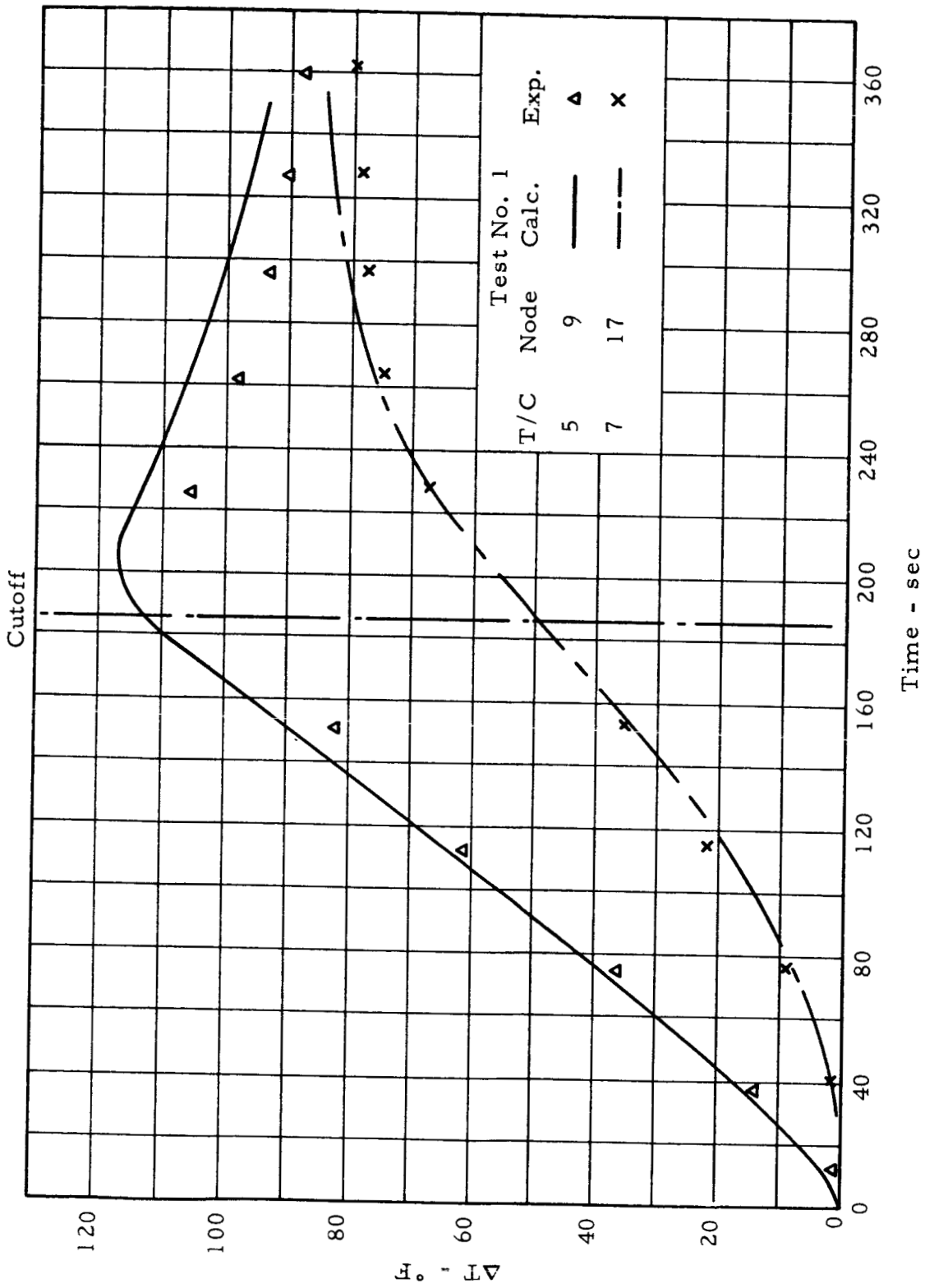
Figure A-3. Temperature Time History (Nodes 9 and 17, Test No. 1)

Figure A-4. Temperature Time History (Nodes 501, 509, and 513; Test No. 1)
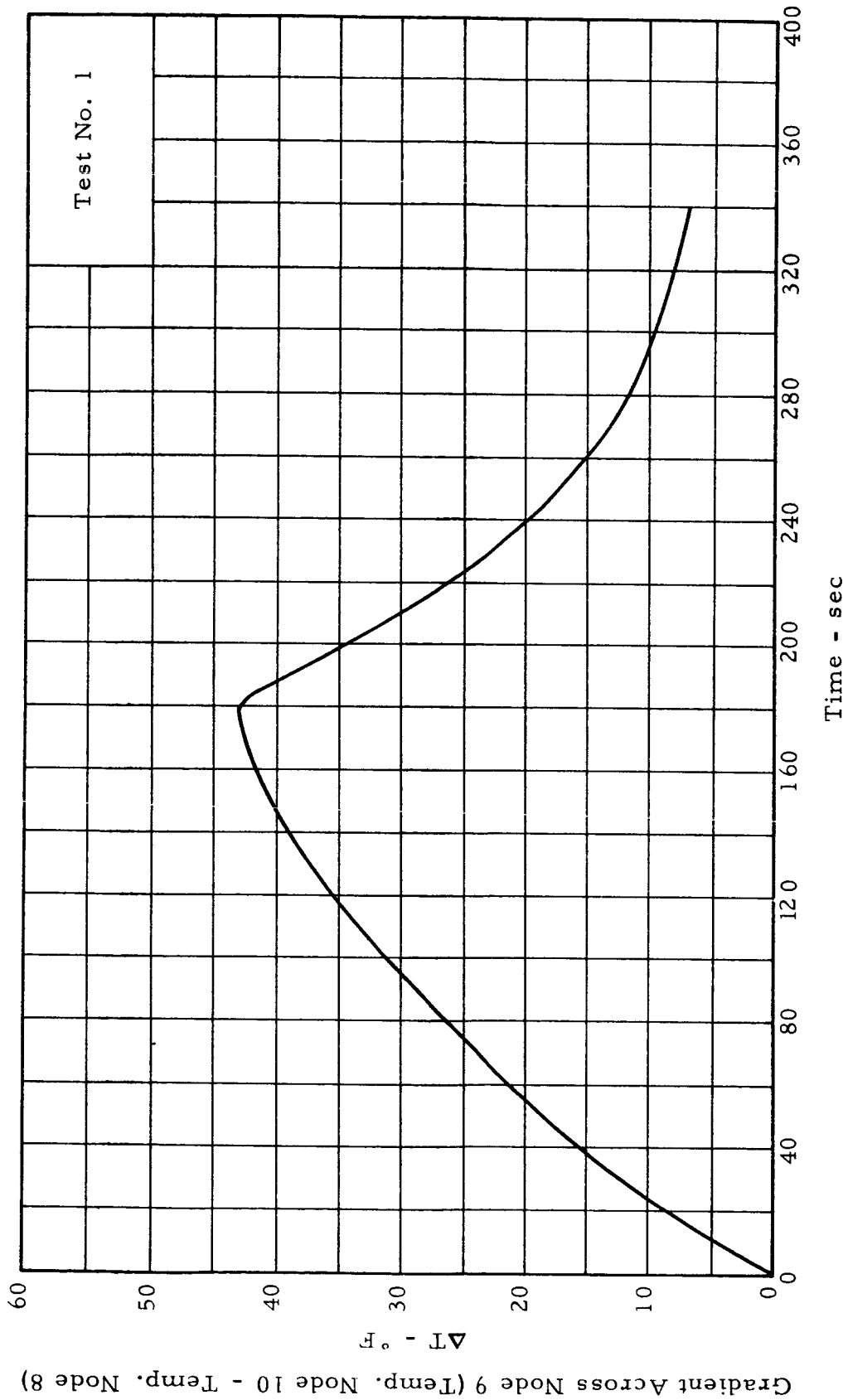
Figure A-5. Gradient Across Node 9 Versus Time

TABLE A-2a

Test No. 2

Experimental

T/C/Node	2/5	4/5	6/13	9/503	10/505
Time/Temp	0/80	0/80	0/80	0/80	0/80
Time/Temp	9/115	11/104	14/80	17/80	18/80
Time/Temp	40/162	43/143	46/85	50/83	51/83
Time/Temp	76/208	79/184	84/95	87/92	88/92
Time/Temp	118/255	117/225	121/109	125/105	126/104
Time/Temp	153/298	157/266	162/128	165/122	166/122
Time/Temp	196/334	199/301	203/148	207/142	208/142
Time/Temp	247/239	250/229	256/164	259/162	260/161
Time/Temp	285/211	288/205	290/167	294/167	295/166
Time/Temp	318/197	321/193	324/168	328/168	329/168
Time/Temp	352/188	354/186	358/168	361/169	362/169
Time/Temp	385/182	389/180	392/169	395/169	396/169

TABLE A-2b

Test No. 2

Calculated

T/C/Node Time	2/5	4/5	6/13	9/503	10/505
0	80	80	80	80	80
20	129.0	129.0	80.7	80.3	80.2
40	155.9	155.9	83.8	82.0	81.7
60	180.9	180.9	88.6	85.6	84.9
80	206.4	206.4	94.6	90.6	89.4
100	232.5	232.5	101.7	96.9	95.2
120	259.4	259.4	109.8	104.3	102.2
140	281.8	281.8	118.9	112.7	112.7
160	302.0	302.0	128.7	122.0	119.0
180	320.2	320.2	138.8	131.9	128.5
200	337.3	337.3	149.3	142.2	138.4
220	292.7	292.7	159.2	152.5	148.5
240	264.6	264.6	166.0	161.0	157.2
260	245.1	245.1	170.1	167.0	163.5
280	229.8	229.8	172.6	170.9	167.9
300	218.2	218.2	174.0	173.3	170.8
320	208.9	208.9	174.9	174.7	172.7
340	202.0	202.0	175.3	175.5	173.8

Figure A-6. Temperature Time History (Nodes 9 and 17, Test No. 2)

Figure A-7. Temperature Time History (Node 3, Test No. 2)

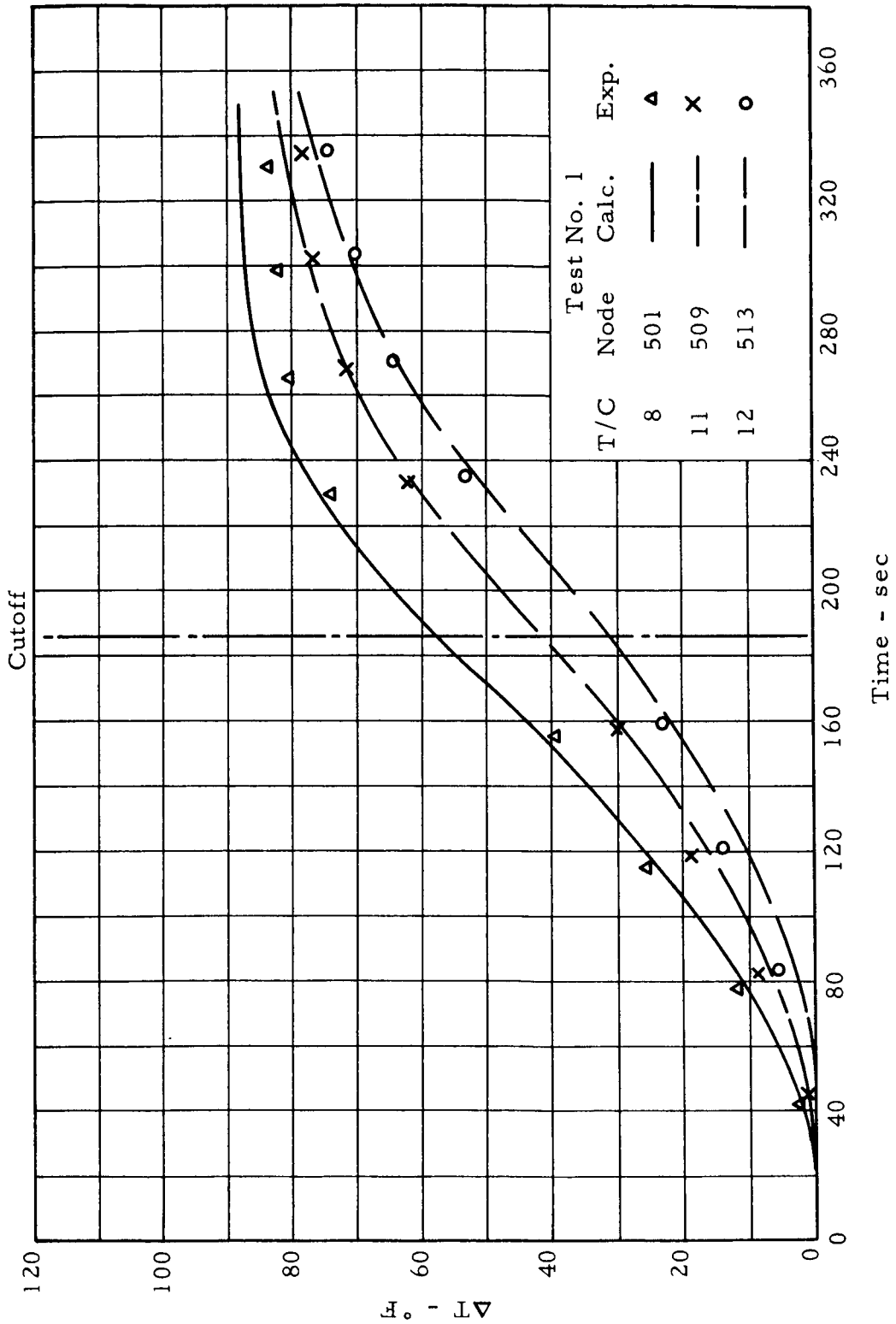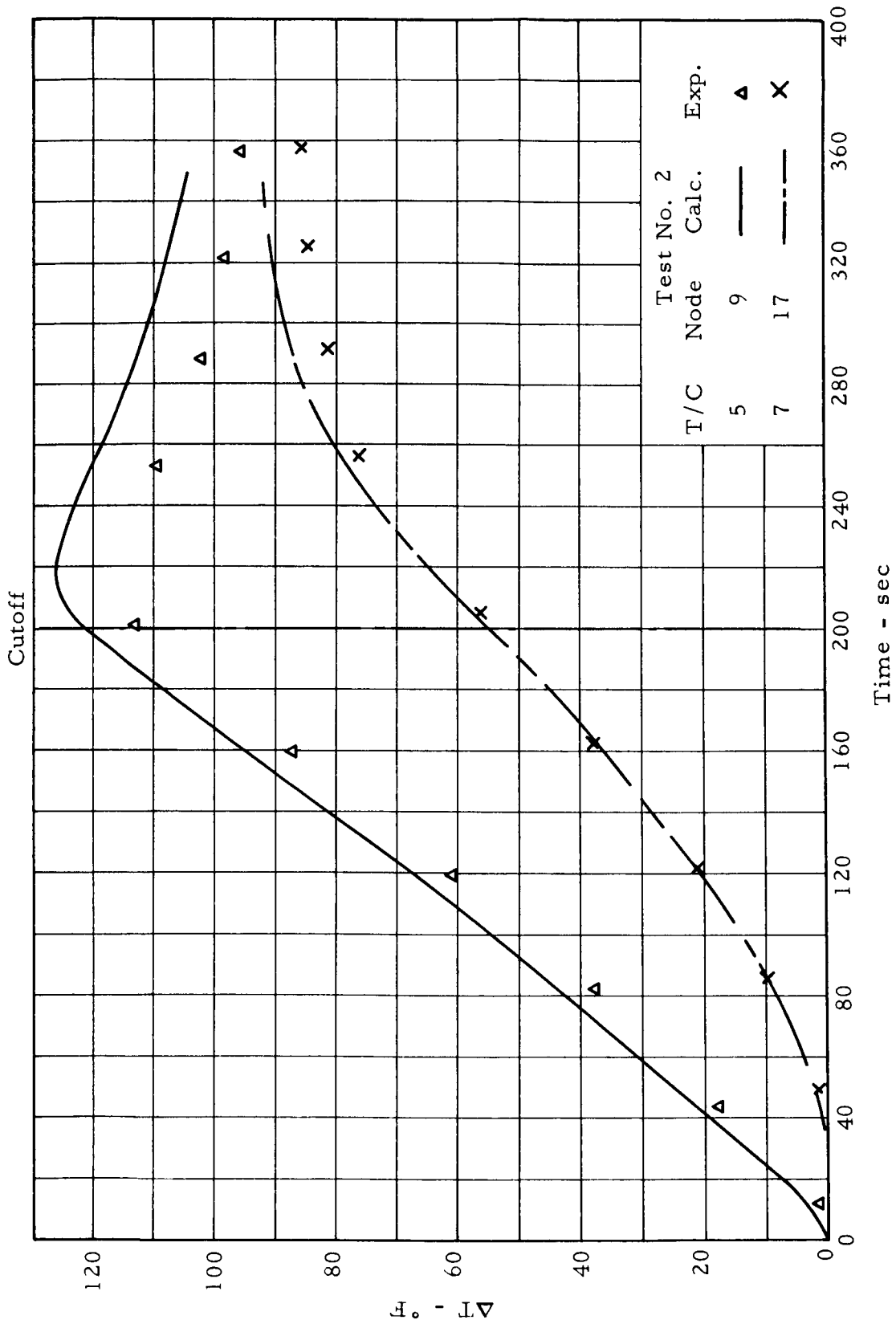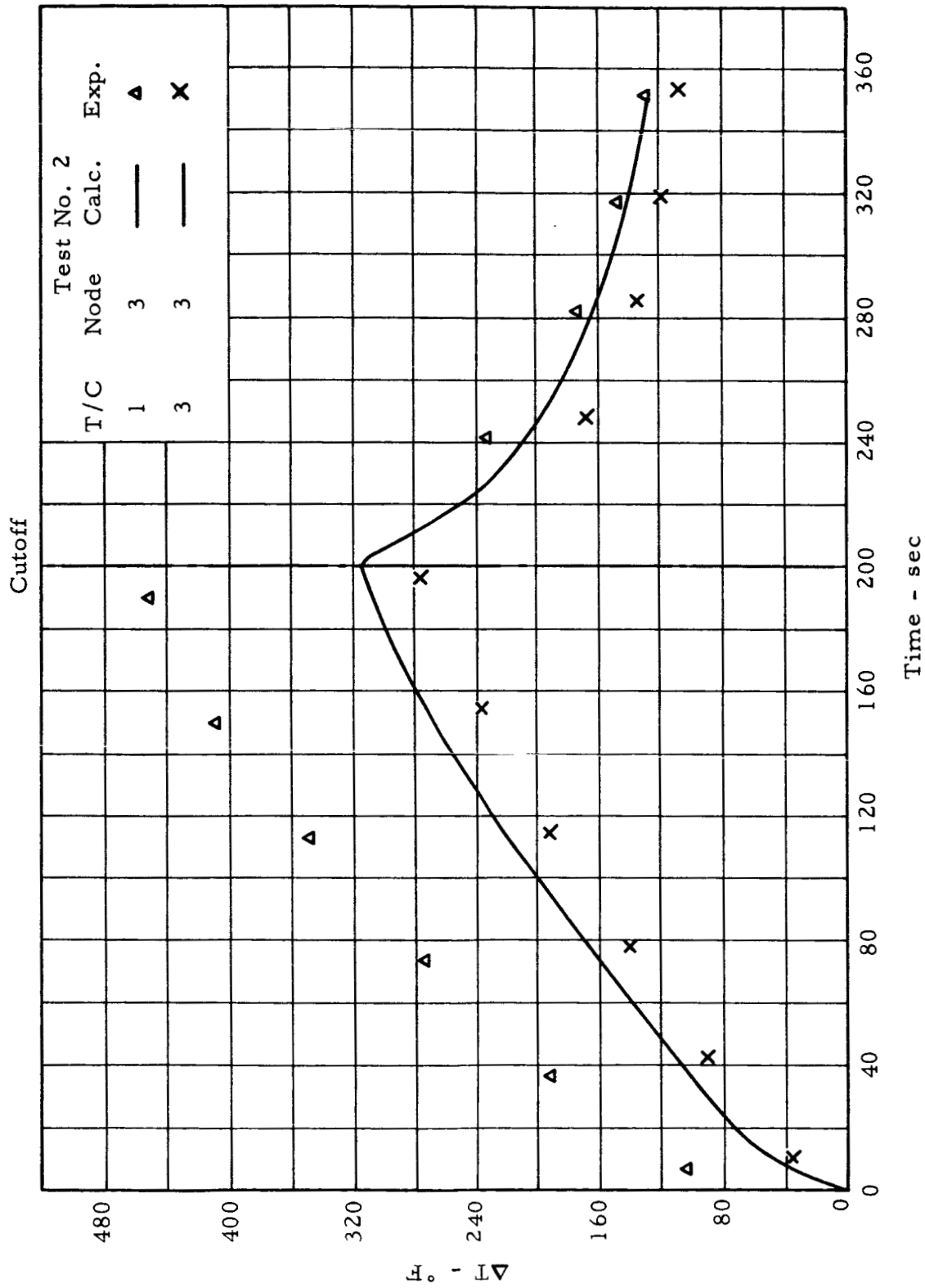Figure A-8. Temperature Time History (Nodes 501, 509, and 513; Test No. 2)
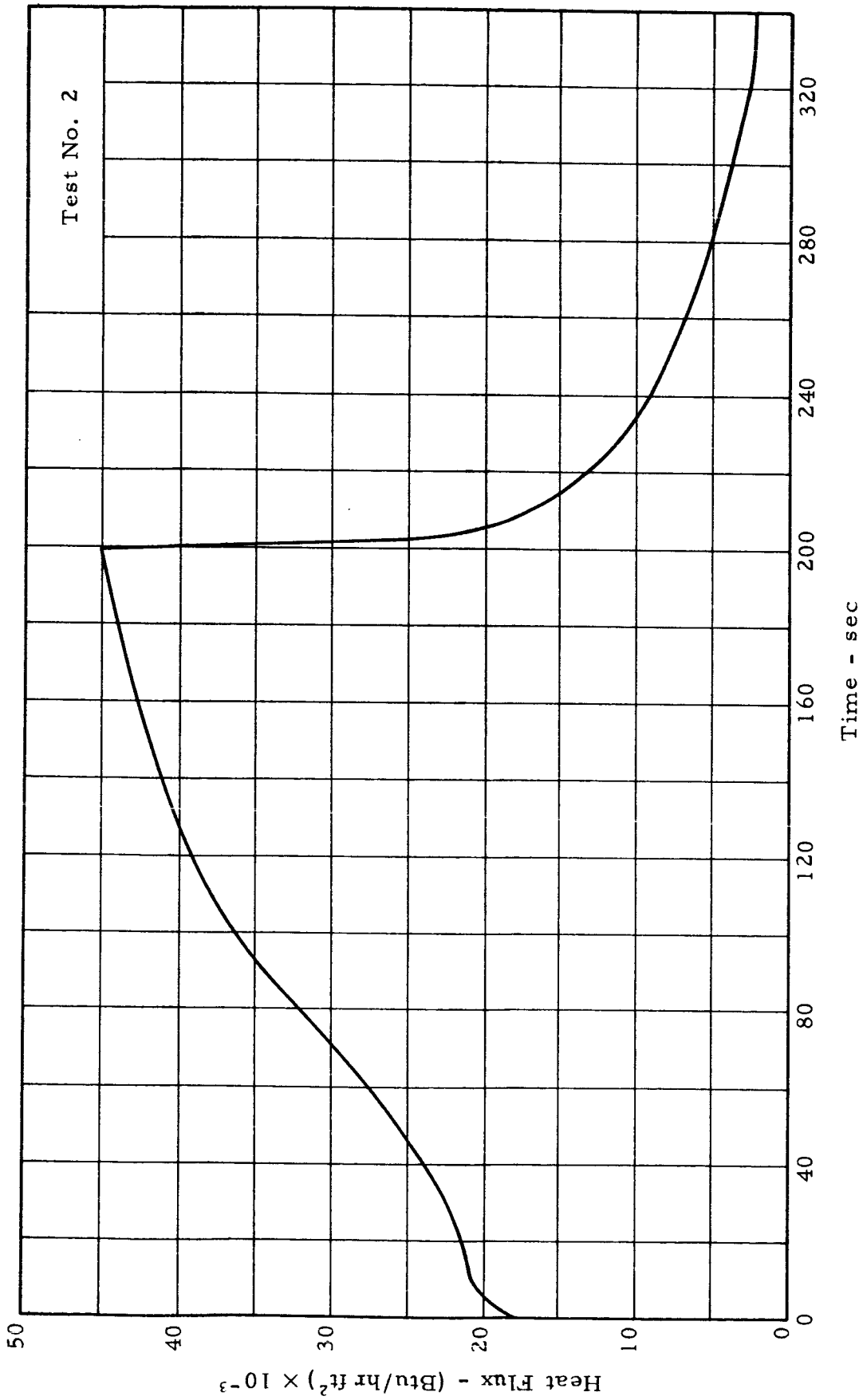
Figure A-9. Total Heat Flux Versus Time (Test No. 2)

TABLE A-3a

Test No. 3

Experimental

T/C/Node	2/5	4/5	6/13	9/503	10/505
Time/Temp	0/89	0/89	0/89	0/89	0/89
Time/Temp	2/100	4/98	7/90	10/89	11/89
Time/Temp	35/161	37/143	40/93	44/91	45/91
Time/Temp	70/209	73/185	77/102	81/99	82/99
Time/Temp	108/258	111/228	115/116	119/111	120/111
Time/Temp	149/301	152/268	158/134	162/129	163/129
Time/Temp	193/338	197/306	202/155	207/150	208/150
Time/Temp	250/250	253/239	257/174	262/172	263/171
Time/Temp	288/220	290/215	294/177	298/177	298/176
Time/Temp	326/205	328/201	331/177	335/178	336/178
Time/Temp	362/196	365/194	368/177	371/178	372/178

TABLE A-3b

Test No. 3

Calculated

T/C Node Time	2/5	4/5	6/13	9/503	10/505
0	89.0	89.0	89.0	89.0	89.0
20	134.1	134.1	89.6	89.3	89.2
40	160.0	160.0	92.5	90.9	90.6
60	186.0	186.0	97.0	94.2	93.5
80	214.0	214.0	102.8	99.0	97.9
100	241.5	241.5	109.9	105.2	103.6
120	267.7	267.7	118.1	112.6	110.4
140	289.9	289.9	127.2	121.0	118.4
160	309.5	309.5	137.0	130.3	127.3
180	326.6	326.6	147.1	140.2	136.8
200	342.0	342.0	157.4	150.4	146.7
220	302.5	302.5	167.4	160.6	156.7
240	274.0	274.0	174.4	169.3	165.4
260	255.3	255.3	178.6	175.4	171.9
280	239.1	239.1	181.1	179.4	176.4

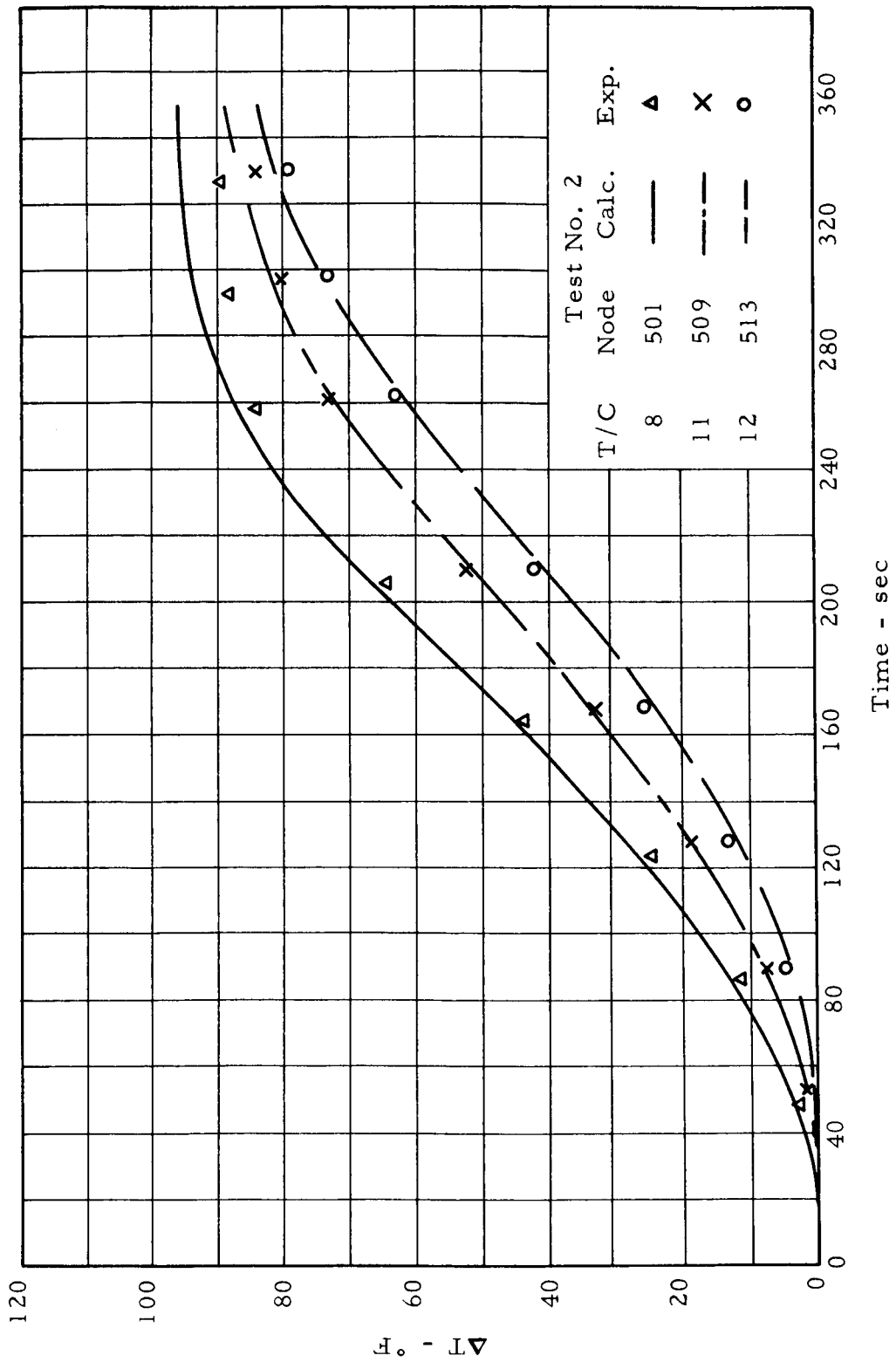Figure A-10.   Temperature Time History (Nodes 9 and 17, Test No. 3)

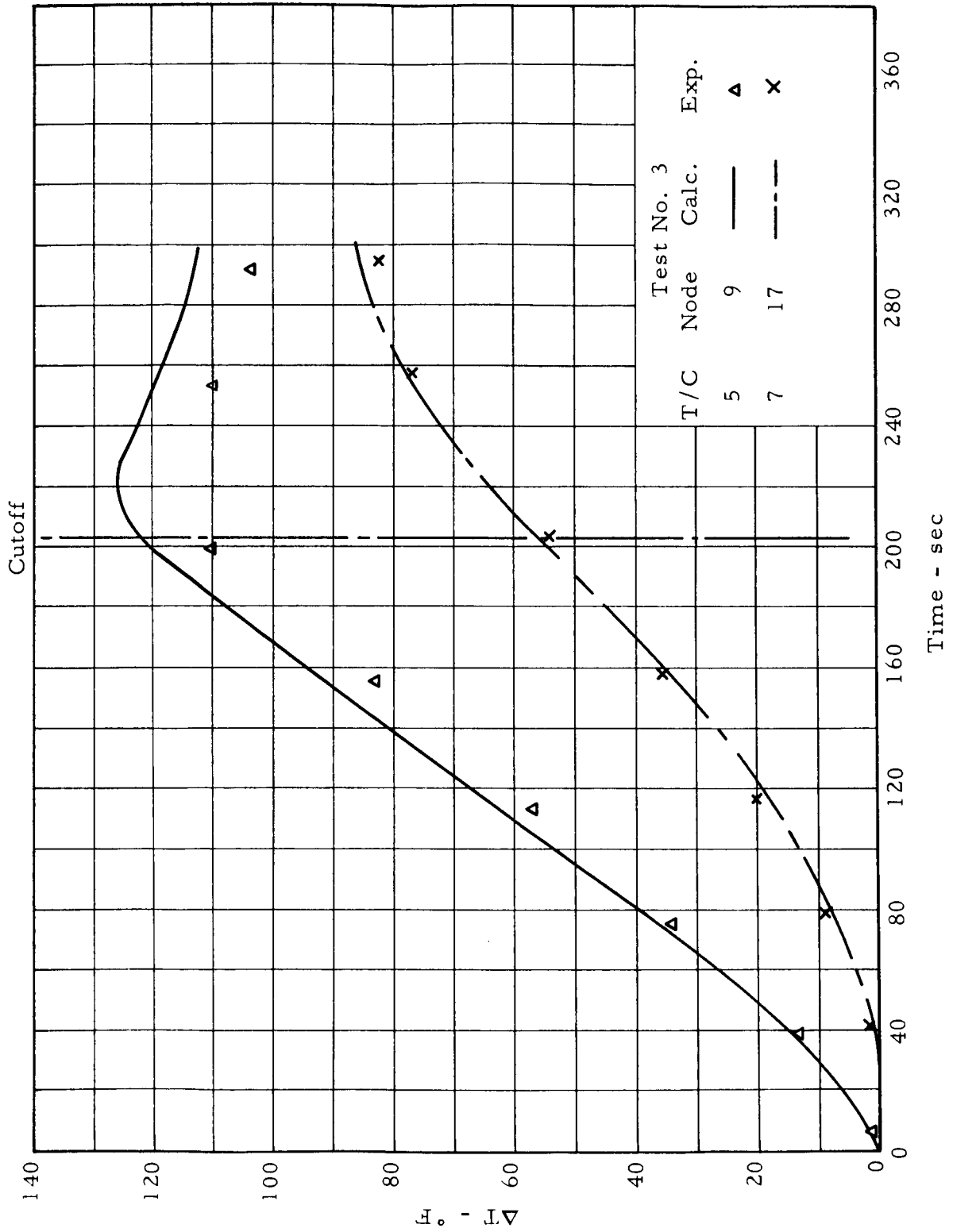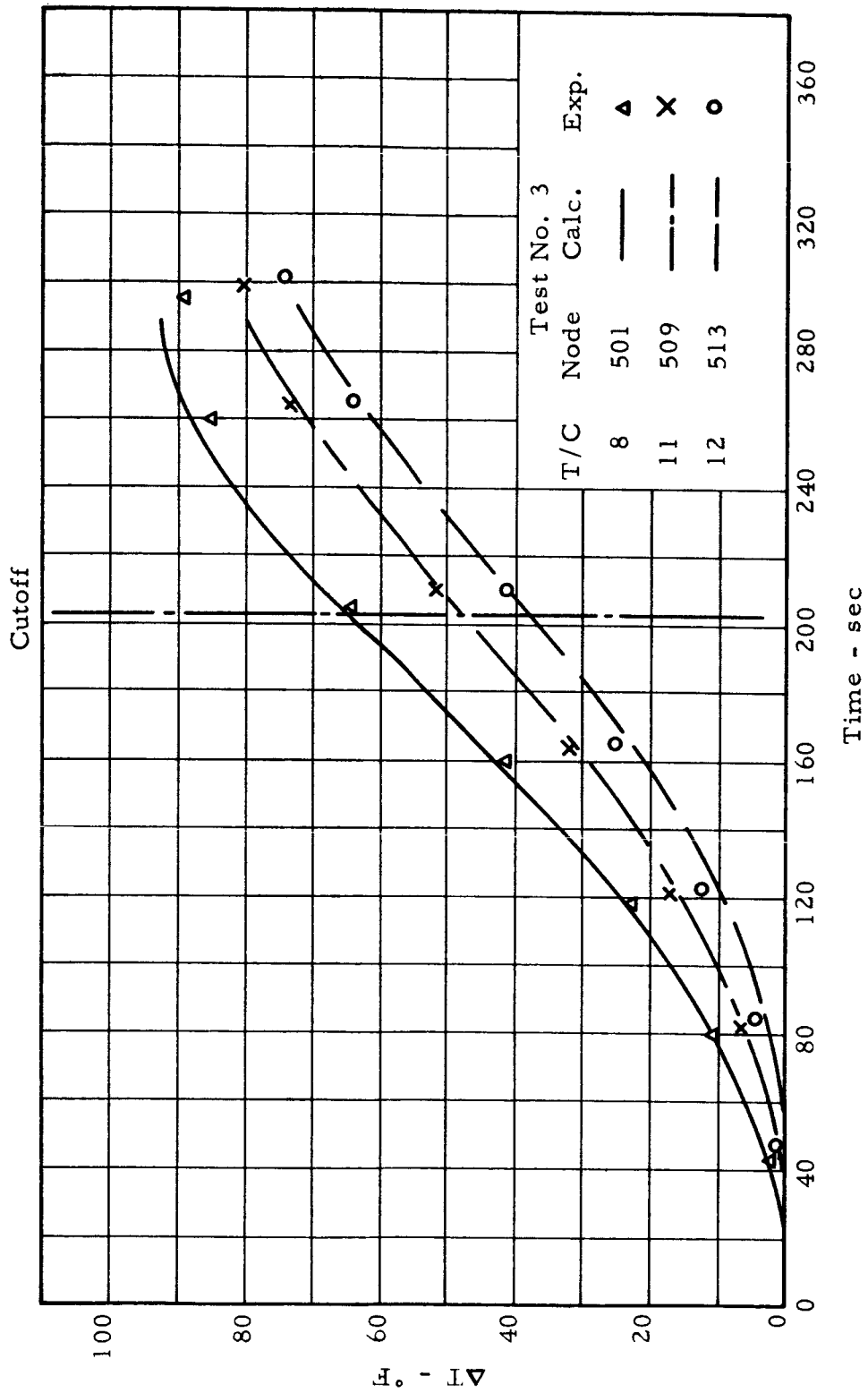Figure A-11. Temperature Time History (Nodes 501, 509, and 513; Test No. 3)

Figure A-12. Total Heat Flux Versus Time (Test No. 3)

Figure A-13. Temperature Time History (Node 3, Test No. 3)

47

TABLE A-4a

Test No. 4

Experimental

T/C/Node	2/5	4/5	6/13	9/503	10/505
Time/Temp	0/79	0/79	0/79	0/79	0/79
Time/Temp	2/95	4/91	7/80	10/80	11/80
Time/Temp	32/150	35/134	39/83	43/82	44/82
Time/Temp	67/190	70/169	75/92	79/90	80/90
Time/Temp	109/246	112/216	117/105	121/101	122/101
Time/Temp	150/288	153/256	158/123	163/119	164/118
Time/Temp	194/325	197/292	201/145	206/140	207/139
Time/Temp	237/239	240/228	245/159	251/158	252/157
Time/Temp	278/207	281/201	284/162	288/162	289/162
Time/Temp	316/193	318/187	321/163	325/164	326/164

TABLE A-4b

Test No. 4

Calculated

T/C / Node Time	2/5	4/5	6/13	9/503	10/505
0	79.0	79.0	79.0	79.0	79.0
20	126.4	126.4	79.7	79.3	79.2
40	147.2	147.2	82.7	81.0	80.7
60	170.5	170.5	87.0	84.3	83.6
80	198.4	198.4	92.4	88.9	87.8
100	226.9	226.9	99.1	94.7	93.1
120	253.3	253.3	107.1	101.8	99.8
140	277.1	277.1	116.0	110.0	107.5
160	297.8	297.8	125.7	119.2	116.2
180	317.1	317.1	135.9	129.0	125.6
200	312.5	312.5	146.4	139.3	135.6
220	276.5	276.5	155.5	149.2	145.3
240	251.8	251.8	161.4	156.9	153.3
260	233.7	233.7	164.9	162.3	159.0
280	220.0	220.0	167.1	165.7	162.9
300	210.1	210.1	168.4	167.8	165.5
320	202.3	202.3	169.2	169.1	167.2
340	195.5	195.5	169.7	169.8	168.3

Figure A-14. Temperature Time History (Nodes 501, 509, and 513; Test No. 4)

Figure A-15. Temperature Time History (Node 3, Test No. 4)

51

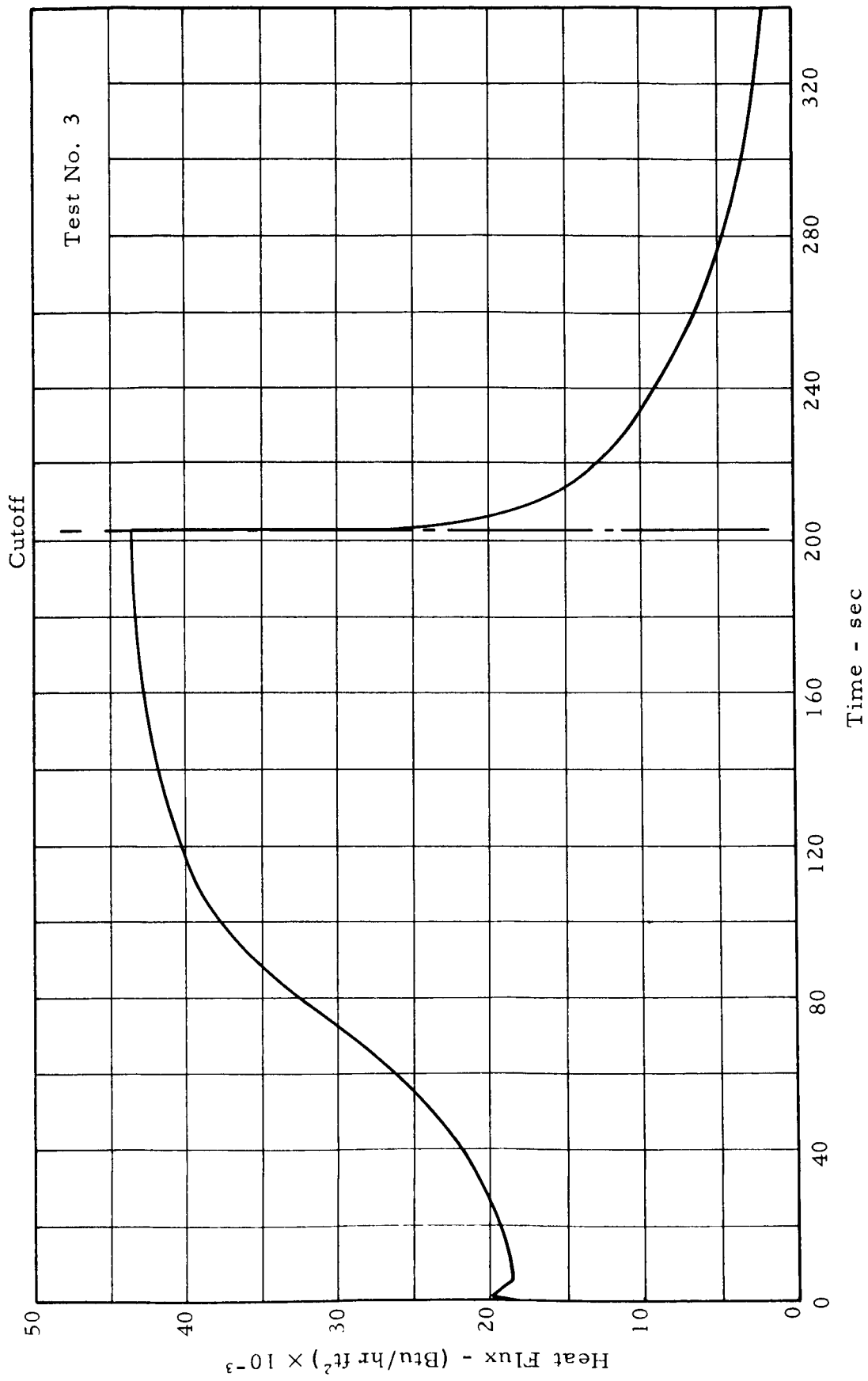Figure A-16. Temperature Time History (Nodes 9 and 17, Test No. 4)

52

Figure A-17. Total Heat Flux Versus Time (Test No. 4)
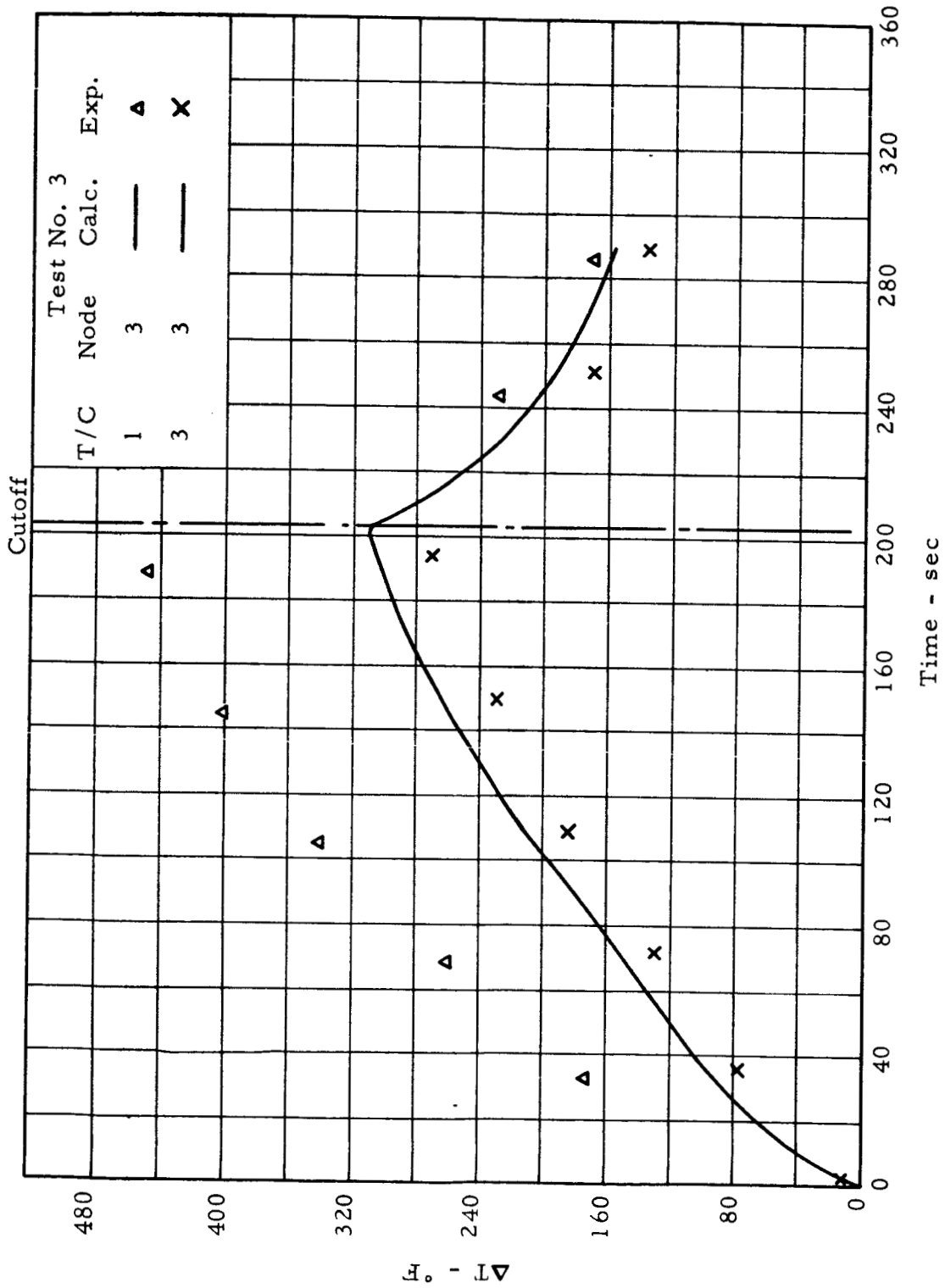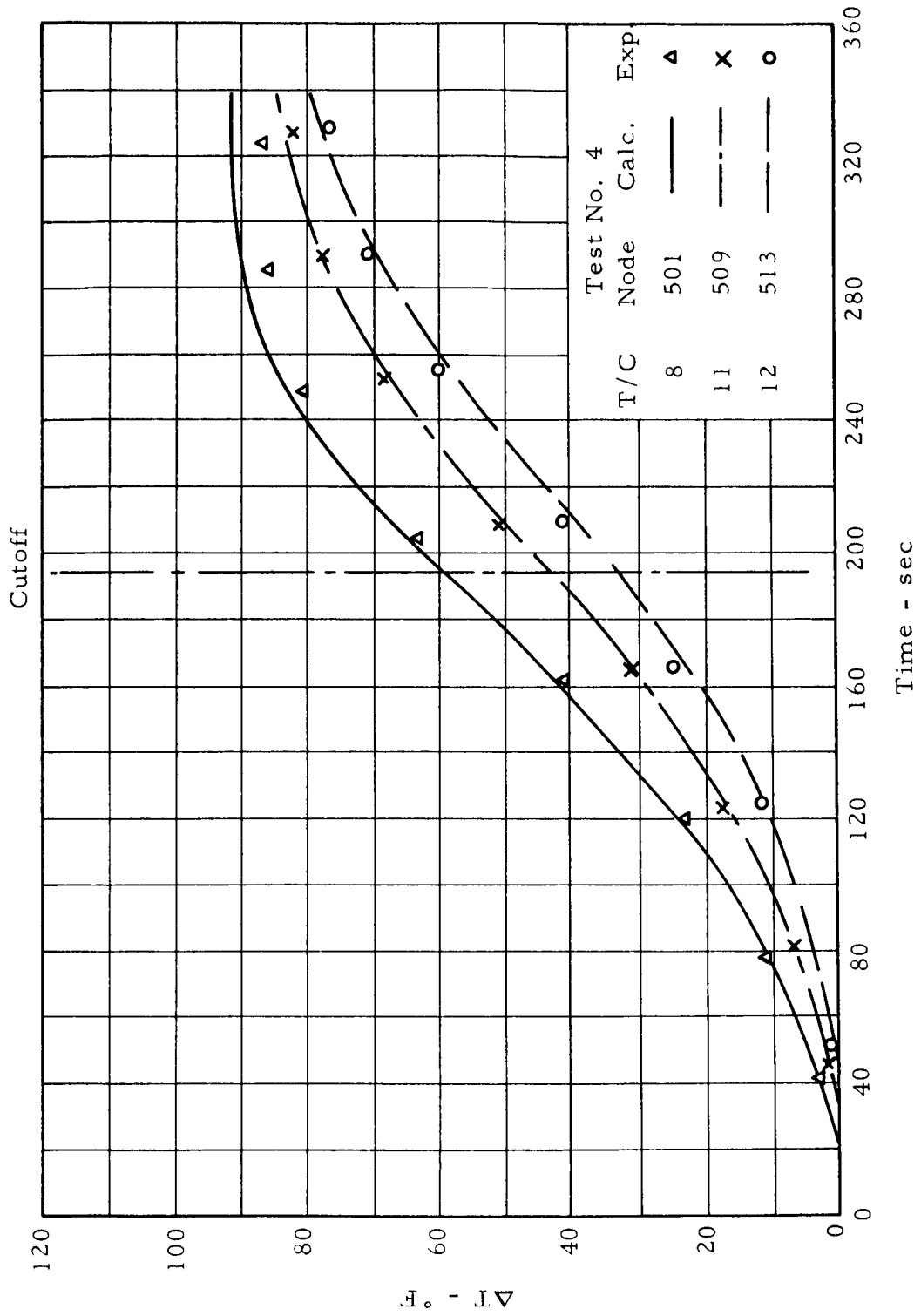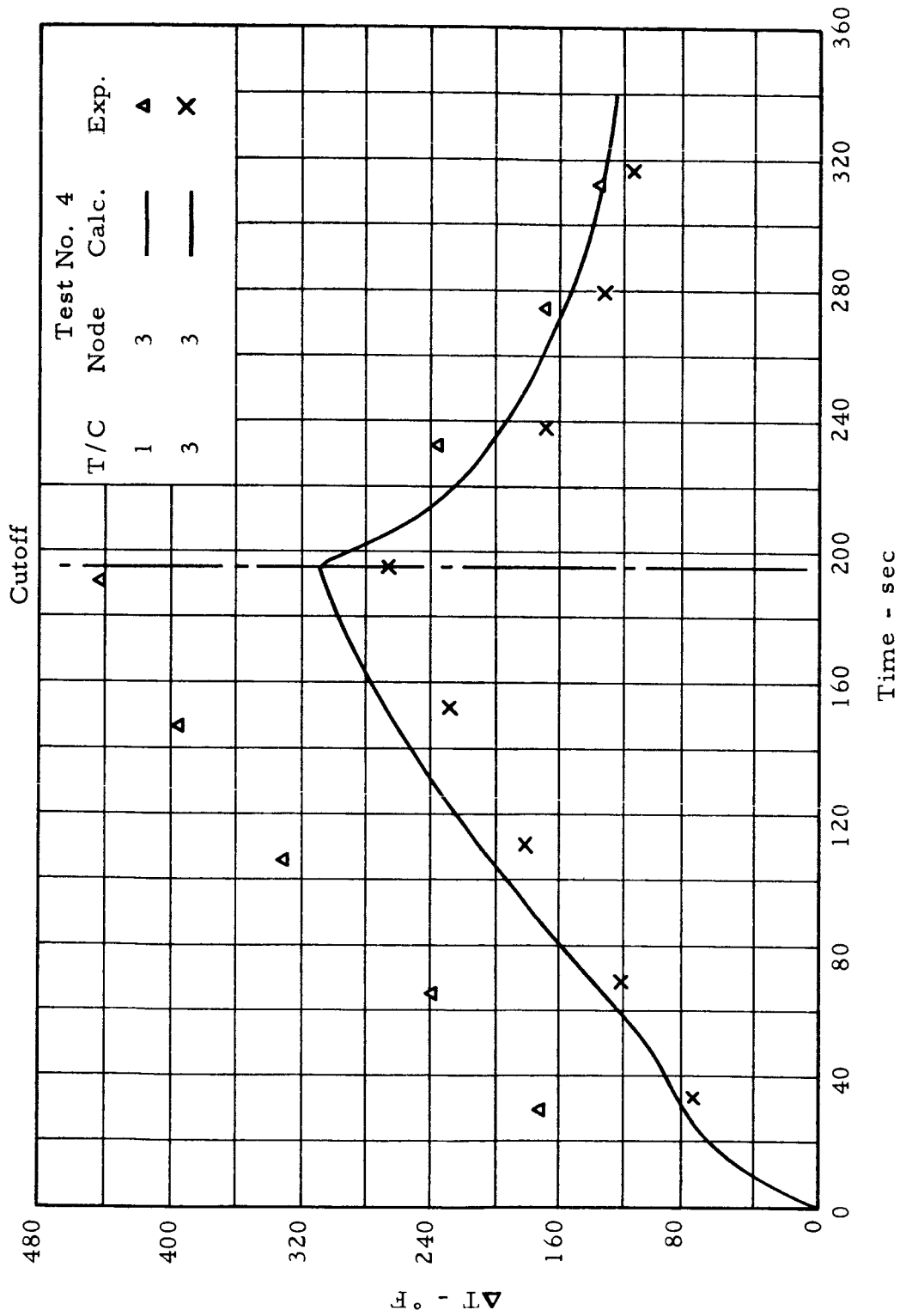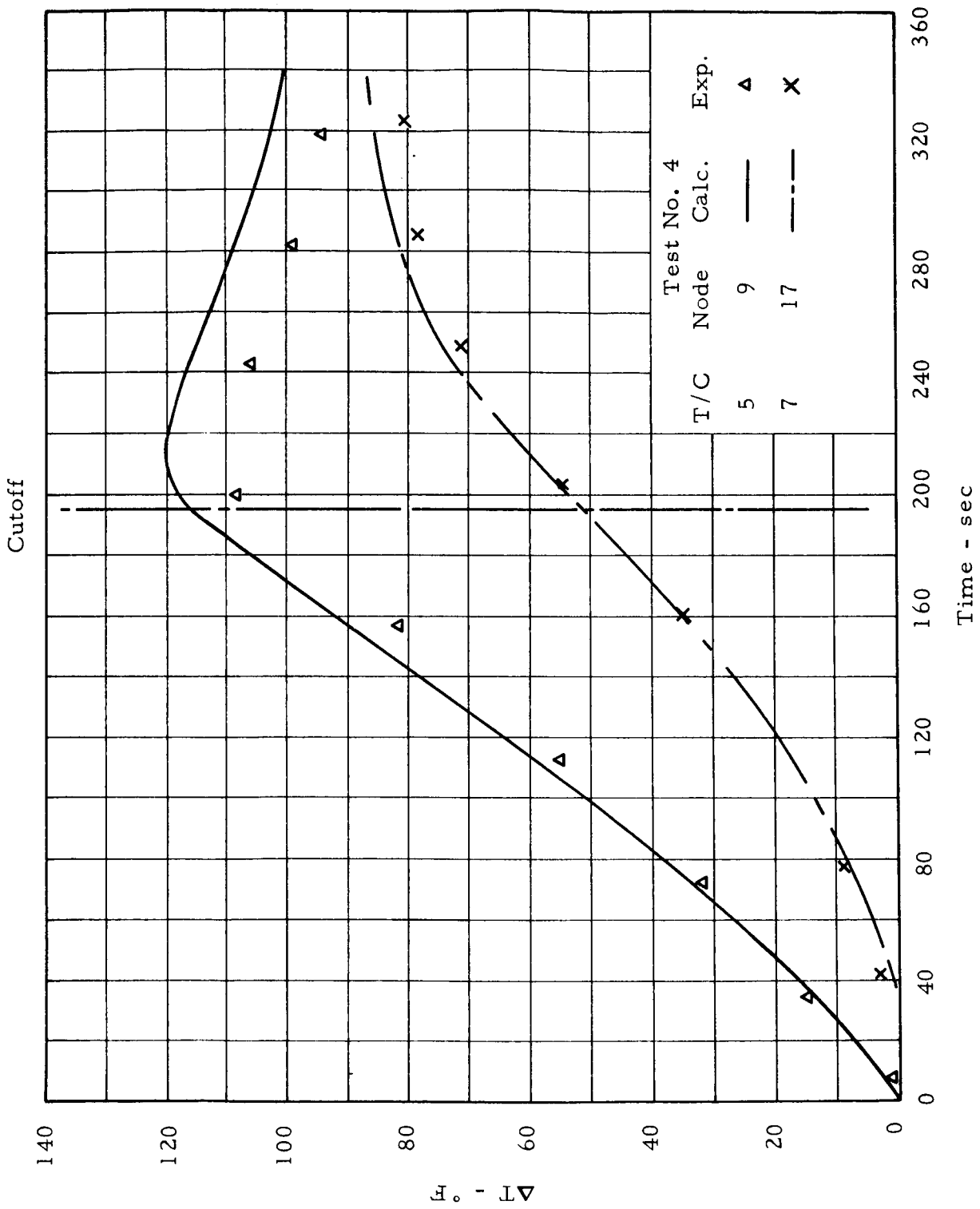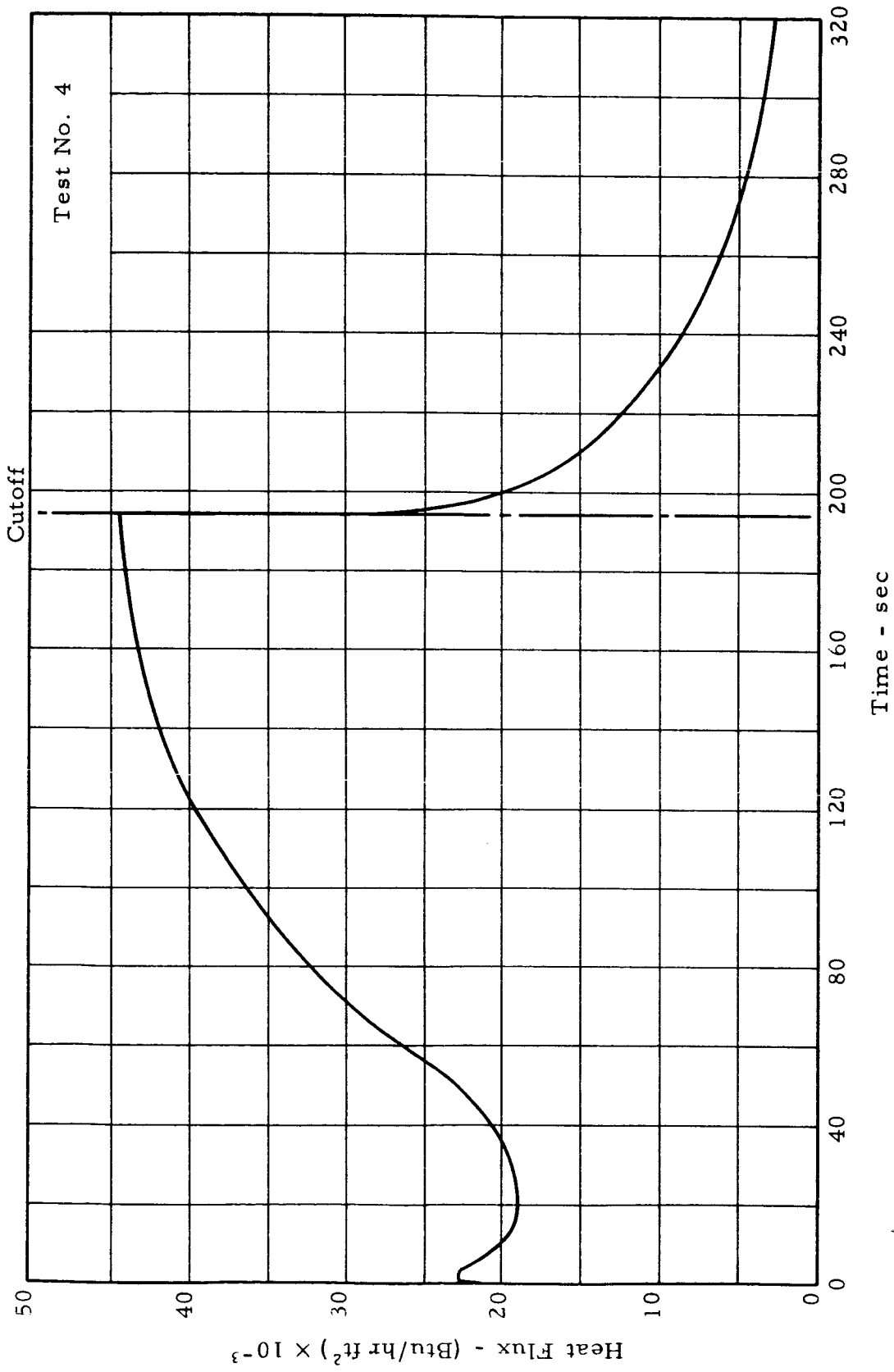
Test No. 4

Cutoff

Time - sec

Heat Flux - (Btu/hr ft^2) $\times$ 10^{-3}

53

APPENDIX B

SHAPE FACTOR ANALYSIS

In order to establish the approximate effect of a change in emissivity of the surface surrounding the heat sensor, heat transfer models were chosen and analyses were made for each case. The model chosen to represent the situation of equal emissivity of the sensor and its surrounding area was a two-inch square box with four reflecting walls to represent the aluminum-lined shaft walls and two black-body ends to represent the blacked sensor and its surrounding area and the open end of the shaft. An equivalent electrical network for this model is depicted in Figure B-1. In this network, E_1 and E_2 are the black-body emissive powers of the bottom (sensor end) and top of the box respectively and E_3, E_4, E_5, and E_6 represent the black-body emissive powers of the sides of the box. Since the ends of the box have been assumed to be black bodies, resistance $R_1 = \rho_1 / A_1 \varepsilon_1$ and $R_2 = \rho_2 / A_2 \varepsilon_2$ are both zero and can be eliminated from the circuit. The sides are identical making R_3, R_4, R_5, and R_6 the same and equal to $\rho / A\varepsilon$. Resistance R_7 through R_{21} are of the form $1/A_m F_{m-n}$ and are equal since the areas and shape factors for all faces are equal. In the expression $1/A_m F_{m-n}$, A_m is the area of any surface and F_{m-n} is the geometric shape factor between surface m and any other surface n based upon area A_m.

A further simplification can be made by recognizing the potentials E_3, E_4, E_5, and E_6 to be equal. The simplified circuit is represented in Figure B-2. In this figure,

$$R_a = R_3 = R_4 = R_5 = R_6 \;,$$

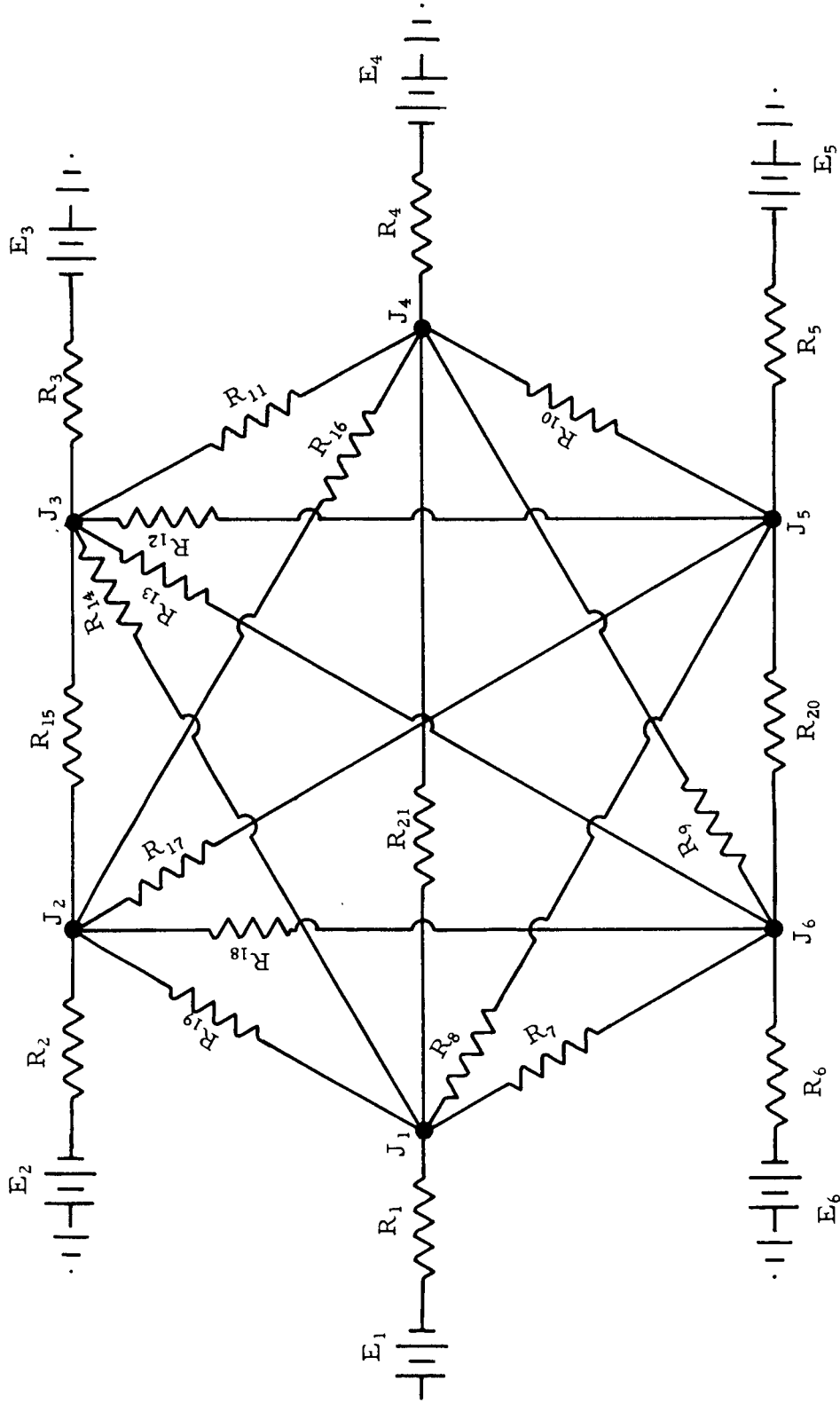$$R_b = R_7 \text{ through } R_{21} \;,$$

55

Figure B-1. Equivalent Network for Case of Equal Emissivity of Sensor and Surrounding Area
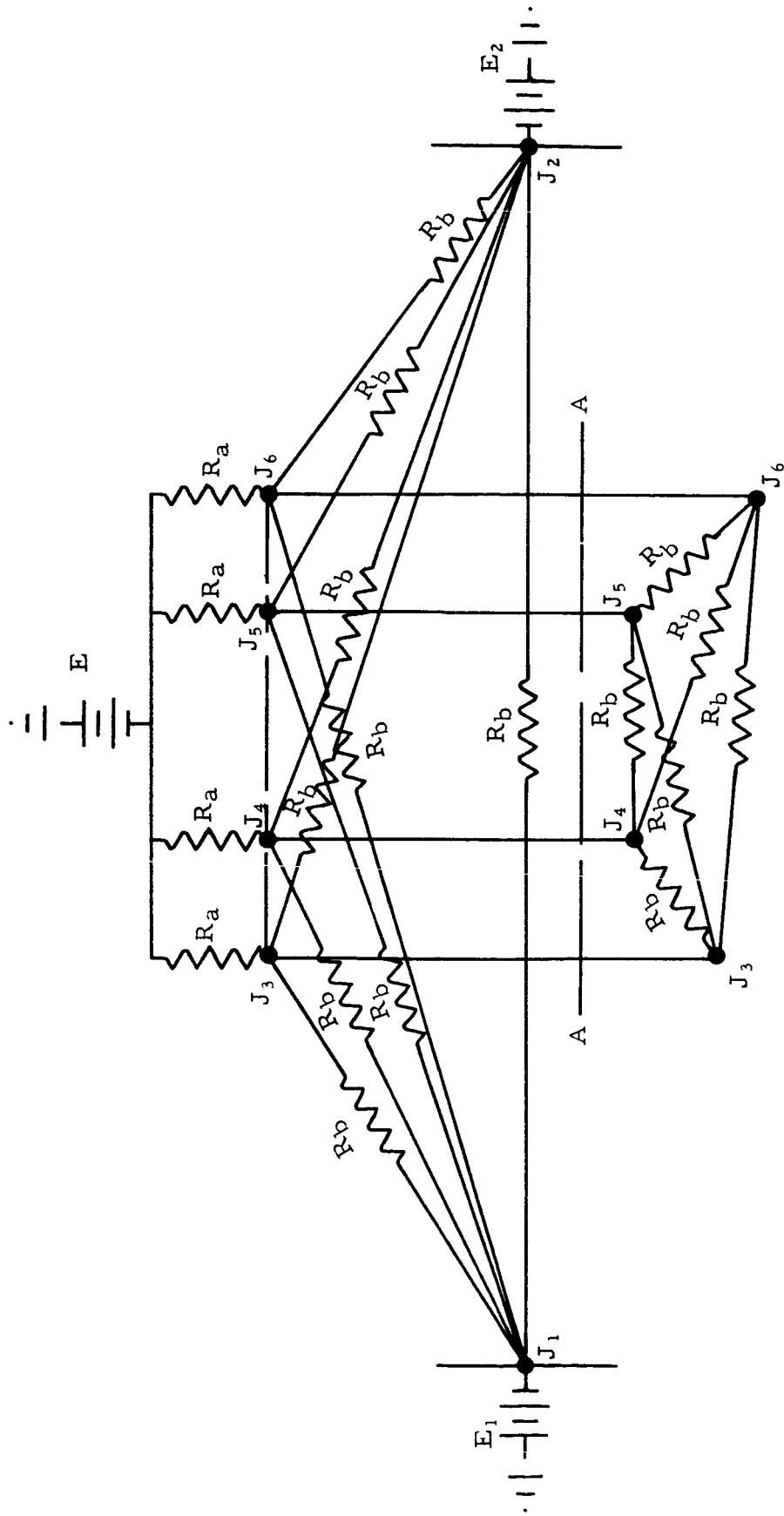
56

Figure B-2. Simplified Network for Case of Equal Emissivity of Sensor
and Surrounding Area

E_1 and E_2 represent the bottom and top of the box respectively as in Figure B-1, and

$$E = E_3 = E_4 = E_5 = E_6 \ .$$

A further simplification of the network can be made by noting that an equipotential line exists passing through junctions J_3, J_4, J_5, and J_6 (dashed line in Figure B-2). Since these junctions are equipotential, the part of the circuit below section A-A plays no functional part in the network. Elimination of this part of the circuit, and recognizing the remaining legs to be three sets of four parallel resistances yields the following final simplification:
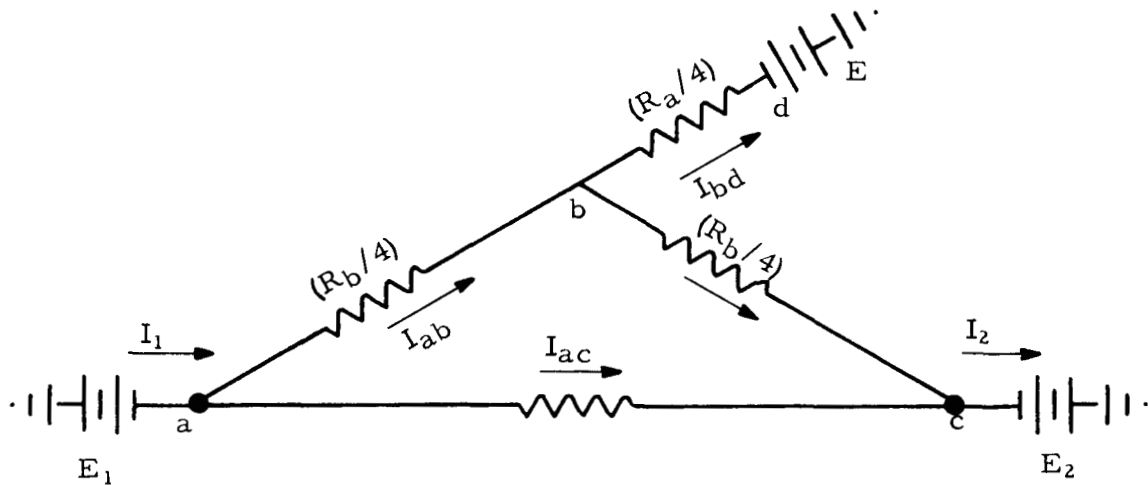

Figure B-3. Final Simplification of Figure B-1

Summation of voltages along the various paths of the system yields the following:

Path a-c-a

$$I_{ac} R_b = E_1 - E_2 \tag{1}$$

58

Path a-b-c

$$I_{ab} \frac{R_b}{4} + I_{bc} \frac{R_b}{4} = E_1 - E_2 \qquad (2)$$

Path a-b-d

$$E_1 - I_{ab} \frac{R_b}{4} - I_{bd} \frac{R_a}{4} - E = 0 \qquad (3)$$

but $I_{bd} = I_{ab} - I_{bc}$, so

$$I_{ab} \left(\frac{R_b}{4} + \frac{R_a}{4} \right) - I_{bc} \frac{R_a}{4} = E_1 - E \qquad (3a)$$

Also,

$$I_1 = I_{ac} + I_{ab} \qquad . \qquad (4)$$

Equations 1, 2, 3a, and 4 can be solved simultaneously to yield

$$I_1 = 4 [(E_1 - E_2) R_a + (E_1 - E) R_b] \frac{1}{2 R_a R_b + R_b^2} + \frac{E_1 - E_2}{R_b} \qquad . \qquad (5)$$

A simplification of the above equation can be made by an order of magnitude comparison of the potentials E_1, E_2, and E. An examination of Reference 3 has yielded an estimation of the temperature of the lamps at 208 volts to be approximately 3500°R. The experimental data indicate that a maximum temperature for the specimen was approximately 1000°R, while the walls were at a slightly lower temperature of about 800°R. A comparison of the potential differences then yields the following:

$$E_1 - E_2 = \sigma T_1^4 - \sigma T_2^4 = \sigma (1^4 - 3^4) \times 10^{12} = -\sigma \, 80 \times 10^{12}$$

$$E_1 - E = \sigma T_1^4 - \sigma T^4 = \sigma (1^4 - 0.8^4) \times 10^{12} = \sigma \, 0.59 \times 10^{12} \quad .$$

It can be seen that the difference $E_1 - E$ may be neglected compared to $E_1 - E_2$. Equation 5 may now be written as

$$I_1 = \left(\frac{4\,R_a}{2\,R_a\,R_b + R_b{}^2} + \frac{1}{R_b}\right)\left(E_1 - E_2\right) \quad . \tag{6}$$

The model chosen to represent the case of different emissivities of the sensor and surrounding area was identical to the previously described model with the exception of the sensor end of the box. This end was broken into two areas. The sensor was allowed to remain a black body and the surrounding surface was treated as a reflecting surface. For this model, Figure B-2 is replaced by Figure B-4. The black body emissive powers of the sensor, top of the box, and area surrounding the sensor are represented by E_1, E_2, and E_3, respectively. The black body emissive powers of the sides are represented by E as in the previous case. It will be noted that the resistances represented by R_a and R_b in Figure B-4 are identical to their counterparts in Figure B-2 but that the resistance represented by R_c and R_d have changed. In addition, resistances R_e, R_f, and R_g have been added to the circuit.

As was the case with the first circuit, it can be seen that an equipotential line exists through junctions 3, 4, 5, and 6 and that the portion of the circuit between sections A-A and B-B plays no functional part in the circuit. This part of the circuit is again eliminated. In order to simplify the circuit, it is assumed that the temperatures of the sensor surface and the surface of the surrounding area are approximately equal and thus allow $E_1 = E_3$. The circuit can now be depicted as in Figure B-5. Another simplification can now be made by recognizing the combinations of parallel resistors. The four resistors R_d in parallel become $R_d/4$; the four resistors R_b in parallel become $R_b/4$; and the four resistors R_e in parallel become $R_e/4$. The circuit
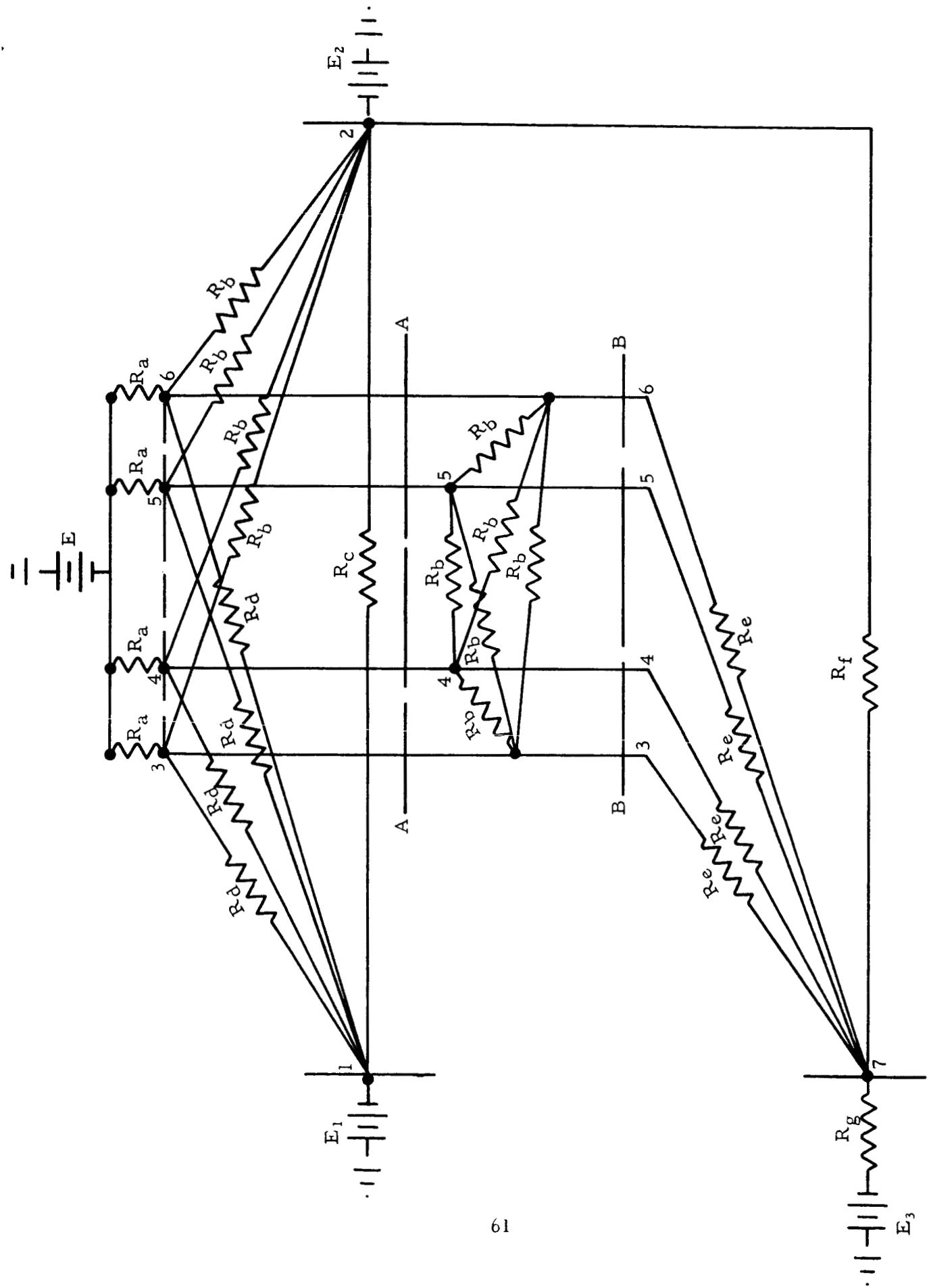
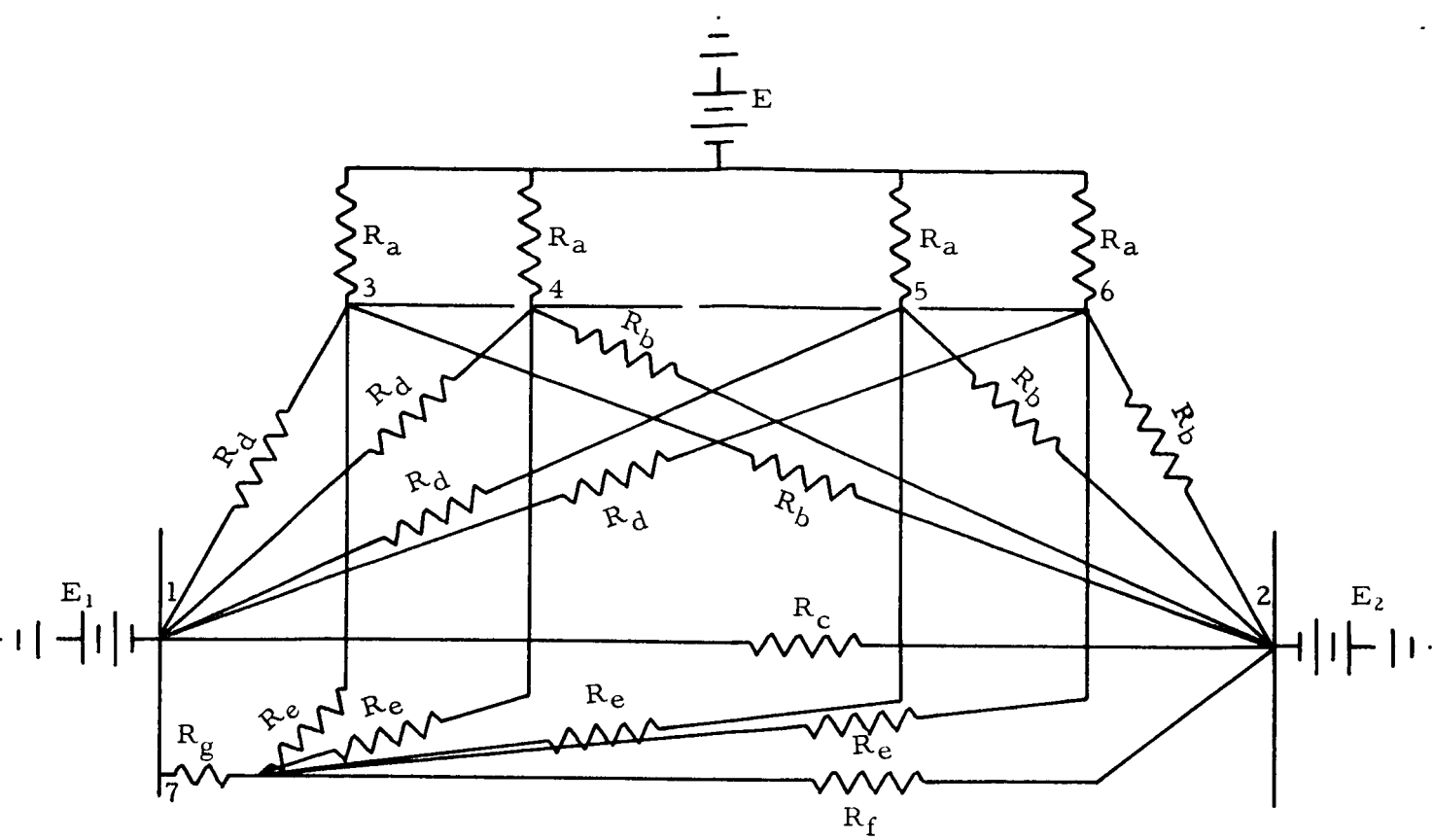Figure B-4. Network for Case of Unequal Emissivity of Sensor and Surrounding Area

61

Figure B-5. Simplification of Network of Figure B-4 by Elimination
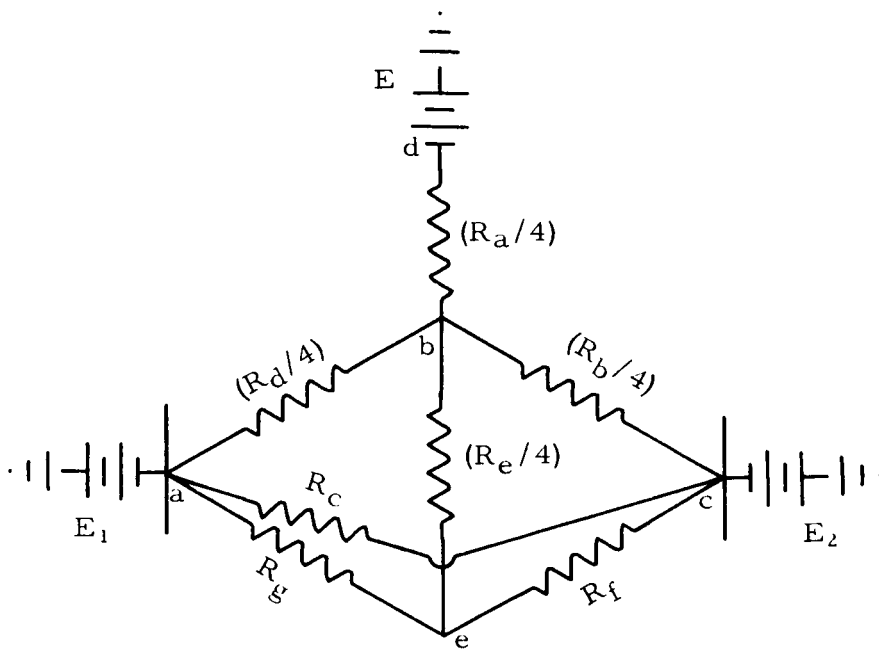of Part of Circuit

Figure B-6. Simplification of Network of Figure B-5 by Utilization
of Combinations of Parallel Resistors

now appears as seen in Figure B-6. A further simplification can be
made by making a transformation of the Δ loop a-b-e to an equivalent
Y circuit. The equations used in the transformation are given in
Reference 4. The equivalent resistances depicted in Figure B-7 are

$$R_x = \frac{(R_d/4)(R_e/4)}{R_g + (R_d/4) + (R_e/4)} = \frac{1}{(16\ R_g/R_d\ R_e) + (4/R_e) + (4/R_d)}$$

$$R_y = \frac{R_g(R_e/4)}{R_g + (R_d/4) + (R_e/4)} = \frac{R_g}{1 + (R_d/R_e) + (4\,R_g/R_e)}$$

$$R_z = \frac{R_g(R_d/4)}{R_g + (R_d/4) + (R_e/4)} = \frac{R_g}{1 + (R_e/R_d) + (4\,R_g/R_d)}$$
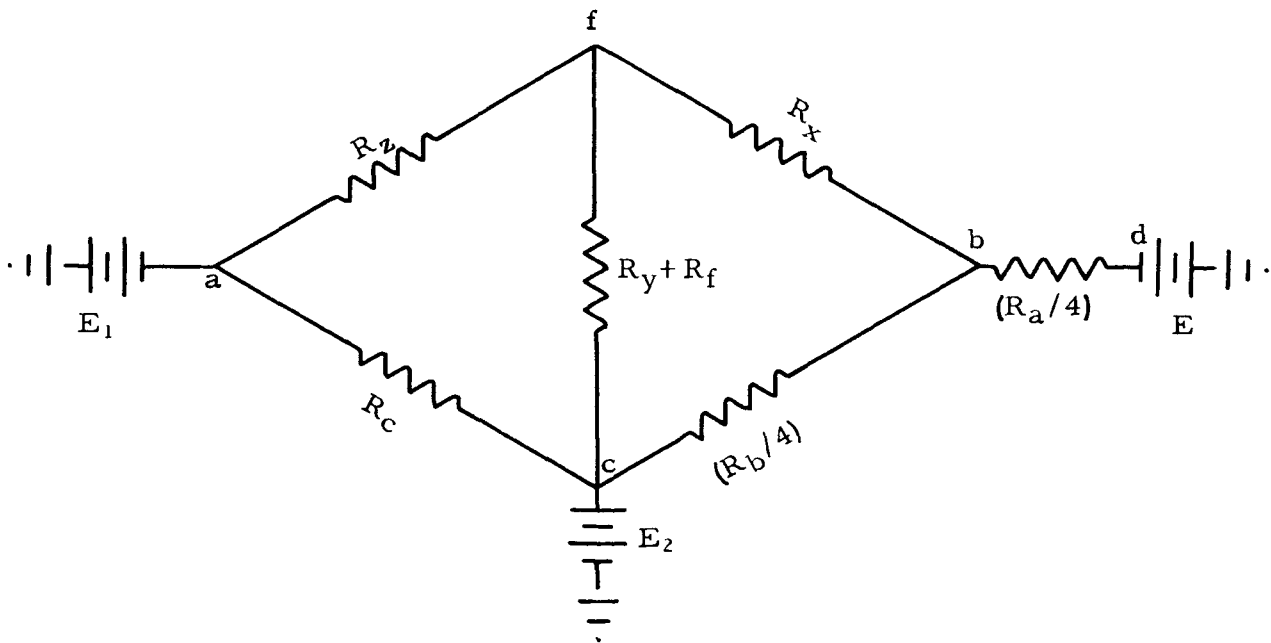
Figure B-7. Circuit of Figure B-6 Modified by Δ-Y
Transformation of Loop a-b-e

63

A final simplification can be made by utilizing a Δ-Y transformation for loop a-c-f in Figure B-7. The resulting circuit is that of Figure B-8 and the resistances R_n, R_m, and R_o are

$$R_n = \frac{R_z(R_y + R_f)}{R_z + R_y + R_f + R_c}$$

$$R_m = \frac{R_z R_c}{R_z + R_y + R_f + R_c}$$

$$R_o = \frac{R_c(R_y + R_f)}{R_z + R_c + R_y + R_f}$$

Figure B-8. Circuit of Figure B-7 Modified by Δ-Y Transformation of Loop a-c-f

It is desired to determine an expression for the current I_1 in terms of a potential difference E_1 - E_2 and an equivalent resistance.

Summation of voltages and currents along the various paths of the
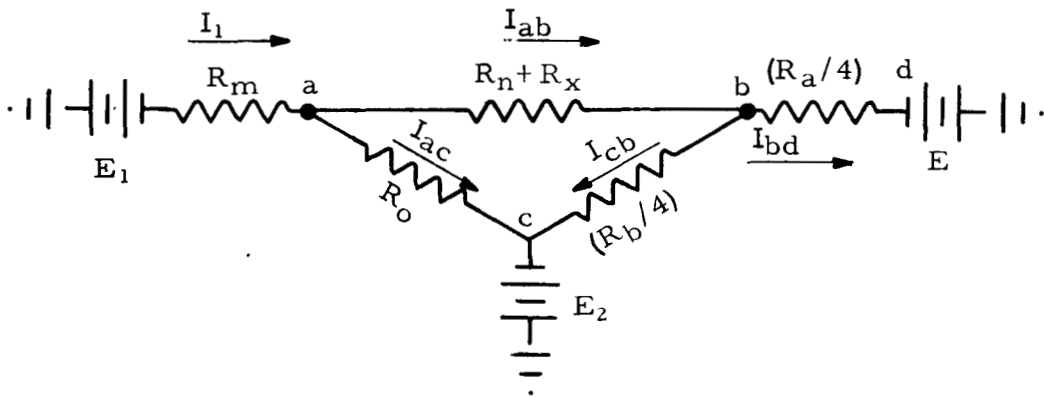circuit yields the following set of equations:

$$I_1 = I_{ab} + I_{ac} \qquad (7)$$

$$I_{bd} = I_{ab} - I_{cb} \qquad (8)$$

Path a-c-a

$$E_1 - I_1 R_m - I_{ac} R_o - E_2 = 0 \qquad (9)$$

Path a-b-d

$$E_1 - I_1 R_m - I_{ab}(R_n + R_x) - I_{bd} \frac{R_a}{4} - E = 0 \qquad (10)$$

Path a-b-c

$$E_1 - I_1 R_m - I_{ab}(R_n + R_x) - I_{cb} \frac{R_b}{4} - E_2 = 0 \qquad . \qquad (11)$$

Solving Equations 8, 10, and 11 simultaneously yields

$$I_{ab} = \frac{(E_1 - E_2)(R_a/4) - I_1\left[(R_m R_a/4) + (R_m R_b/4)\right] + (E_1 - E)(R_b/4)}{(R_n + R_x)(R_a/4) + (R_b/4)\left[R_n + R_x + (R_a/4)\right]} \qquad (12)$$

and Equation 9 yields

$$I_{ac} = \frac{E_1 - E_2}{R_o} - \frac{R_m}{R_o} I_1 \qquad . \qquad (13)$$

As was true with the first model, $(E_1 - E)$ may be neglected when
compared with $(E_1 - E_2)$.

Combining Equations 12 and 13 with Equation 7 then yields

$$I_1 = \frac{\dfrac{E_1 - E_2}{R_o} + \dfrac{(E_1 - E_2)(R_a/4)}{(R_n + R_x)(R_a/4) + (R_b/4)\left[R_n + R_x + (R_a/4)\right]}}{1 + \dfrac{R_m}{R_o} + \dfrac{(R_m R_a/4) + (R_m R_b/4)}{(R_n + R_x)(R_a/4) + (R_b/4)\left[R_n + R_x + (R_a/4)\right]}} \qquad . \qquad (14)$$

The equivalent resistance then is

$$R = \cfrac{1 + \cfrac{R_m}{R_o} + \cfrac{R_m R_a + R_m R_b}{(R_n + R_x)R_a + R_b[R_n + R_x + (R_a/4)]}}{\cfrac{1}{R_o} + \cfrac{R_a}{(R_n + R_x)R_a + R_b[R_n + R_x + (R_a/4)]}}$$ (15)

In order to establish the validity of the above equation, let R_g (the resistance imposed on the circuit by the surface surrounding the sensor) equal zero. This makes $R_y = R_z = R_n = R_m = 0$. The equivalent resistance then becomes

$$R = \cfrac{1}{\cfrac{1}{R_o} + \cfrac{R_a}{R_x R_a + R_b[R_x + (R_a/4)]}}$$ (16)

or

$$R = \cfrac{1}{\cfrac{R_c + R_f}{R_c R_f} + \cfrac{R_a}{[R_a R_e R_d/4(R_d + R_e)] + R_b\{[R_e R_d/4(R_d + R_e)] + (R_a/4)\}}}$$

as compared with

$$R = \frac{2 R_a R_b + R_b^2}{6 R_a + R_b}$$ (17)

for the initial model.

The values for the various resistances were determined by using standard shape factor charts[5,6] and were found to be approximately

$$R_a = 683$$

$$R_b = 180$$

$$R_c = 1270$$

$$R_d = 3000$$

$$R_e = 193$$

$$R_f = 212 \ .$$

Using these values in Equations 16 and 17, the equivalent resistances for the first and second models respectively become 67 and 65. The closeness of these values indicates that the reductions made to arrive at an expression for the second model are correct.

In order to establish the effect of variation of the emissivity of the area surrounding the sensor on the equivalent resistance, Equation 15 should be written in terms of R_g. For the purpose of demonstrating the effect of ε, only values of ε between 0.6 and 1.0 will be used. This allows the various expressions for individual resistances to be simplified to the following:

$$R_y = \frac{R_g}{16.5}$$

$$R_z = R_g$$

$$R_x = 47.5$$

$$R_n = \frac{R_g(0.06\,R_g + 212)}{1.06\,R_g + 1482}$$

$$R_m = \frac{1270\,R_g}{1.06\,R_g + 1482}$$

$$R_o = \frac{1270(0.06\,R_g + 212)}{1.06\,R_g + 1482} \quad .$$

If we assign

$$N = 1.06\,R_g + 1482$$

and

$$M = \left[\frac{R_g}{N}(0.06\,R_g + 212) + 47.5\right]683$$
$$+ \left[\frac{R_g}{N}(0.06\,R_g + 212) + 217\right]180 \quad ,$$

the expression for the equivalent resistance becomes

$$R = \frac{1 + [R_g/(0.06\,R_g + 212)] + [(1.099 \times 10^6\,R_g)/NM]}{\{N/[1270(0.06\,R_g + 212)]\} + (683/M)} \,. \quad (18)$$

The resistance contributed by the area surrounding the sensor is $R_g = \rho/0.0158\,\varepsilon$. Variation of ε from 1.0 to 0.6 yields the curve of Figure B-9. The emissivity of glass rock is in the range of 0.8 to 0.9 and blacking increased the value to the neighborhood of 1.0. Examination of Figure B-9 shows that the decrease in emissivity during a test would cause a significant change in resistance.
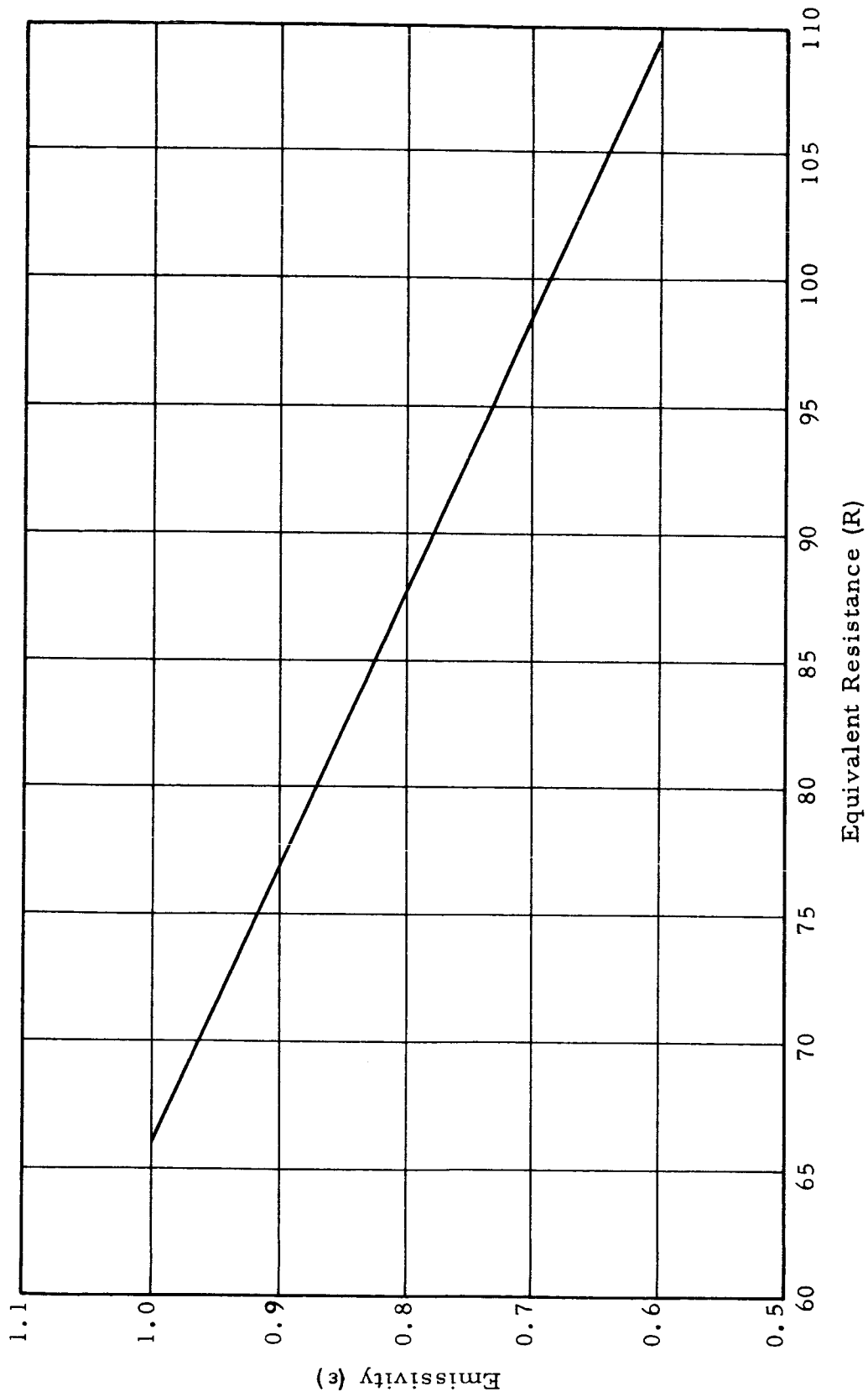
Figure B-9. Equivalent Resistance Versus Emissivity of Surface Surrounding Sensor

DOCUMENT CONTROL DATA - R&D

(Security classification of title, body of abstract and indexing annotation must be entered when the overall report is classified)

1. ORIGINATING ACTIVITY (Corporate author)	2a. REPORT SECURITY CLASSIFICATION
Brown Engineering Company, Inc.	N/A
	2b. GROUP
	N/A

3. REPORT TITLE

Experimental Transient Three-Dimensional Heat Transfer Analysis

4. DESCRIPTIVE NOTES *(Type of report and inclusive dates)*

Technical Note, May, 1965

5. AUTHOR(S) *(Last name, first name, initial)*

Blanton, Dr. Roy W., Jr.
Littles, J. Wayne

6. REPORT DATE	7a. TOTAL NO. OF PAGES	7b. NO. OF REFS
May, 1965	80	6

8a. CONTRACT OR GRANT NO.	9a. ORIGINATOR'S REPORT NUMBER(S)
NAS8-5289	
b. PROJECT NO.	TN R-145
c. NONE	9b. OTHER REPORT NO(S) (Any other numbers that may be assigned this report)
d.	N/A

10. AVAILABILITY/LIMITATION NOTICES

NONE

11. SUPPLEMENTARY NOTES	12. SPONSORING MILITARY ACTIVITY
NONE	N/A

13. ABSTRACT

This report describes the results of a study which was undertaken to compare calculated data from the G.E. General Transient Heat Transfer program with experimental data. The capability of the program to handle a total heat flux input as a function of time was verified.

14. KEY WORDS

Heat transfer
Transient
Experimental
Three-Dimensional
Computer program
Verification